Electric-field control of exciton fine structure in alloyed nanowire quantum dot molecules

Michał Świderski[*] and Michał Zieliński [†]

Institute of Physics, Faculty of Physics, Astronomy and Informatics, Nicolaus Copernicus University, ul. Grudziądzka 5, 87-100 Toruń, Poland

Alloyed $InAs_{0.2}P_{0.8}$/InP nanowire quantum dot molecules reveal nontrivial electric-field evolution of the bright-exciton spectra; this was studied here using the atomistic theory. For a quantum dot molecule composed of two nanowire quantum dots of dissimilar sizes, the overall field dependence resembles the typical self-assembled quantum dot molecule spectra with an avoided crossing of direct and indirect excitons. However, for coupled nanowire quantum dots of identical dimensions and chemical compositions—where the bright-exciton splitting is triggered by alloy randomness—the notion of direct/indirect excitons is mostly lost, with the bright-exciton splitting field evolution varying strongly between various random realizations of nominally identical systems. Nonetheless, for several random samples, lower-higher excitonic branch mixing leads to the reduction of bright-exciton splitting below the 1 μeV threshold but with the restoration of pronounced optical activity away from the crossing. Thus, a simultaneous reduction of the bright-exciton splitting, without the detrimental reduction in the lower excitonic branch optical activity, makes alloyed nanowire quantum dot molecules a possible platform for applications in quantum optics and information.

I. INTRODUCTION

Nanowire quantum dots [1,2] are promising for applications to quantum optics, communication, and information [3–9]. In particular, the vapor-liquid-solid [10,11] (VLS) growth mode of nanowire quantum dots allows for precise spatial positioning and the efficient control of dimensions of individual quantum dots [12–15]. It also enables obtaining high-quality nanowire quantum dots with excellent optical properties [16,17], and it allows the customization of the shape of the host nanowire for efficient light extraction [18,19]. For InAs/InP nanowire quantum dots, the VLS growth intrinsically produces a high concentration of barrier material, leading to the formation of highly alloyed $InAs_{1-x}P_x$ quantum dots with the value of x reaching 80% [17,20]. Such large intermixing has two important effects on the properties of nanowire quantum dots. Its primary effect is a significant reduction in the depth of the confining potential because the conduction and valence band offsets between the $InAs_{0.2}P_{0.8}$ dot and InP barrier are approximately five times smaller than those of the idealized InAs/InP systems [21]. Such shallow confinement increases the energies of excitons confined in nanowire quantum dots and also leads to a pronounced leakage of a single particle into the barrier region with further potential consequences for the excitonic spectra. Second, intermixing inevitably triggers alloy randomness, which strongly impacts the fine structure of the excitonic spectra [22–26].

Although the spectral properties of single-nanowire quantum dots have been relatively well investigated [27], double-nanowire quantum dots have been rarely studied [9,26,28]. Such coupled quantum dots may form a solid-state analog of a molecular system [29,30]—an artificial molecule—with quantum dot separation (interdot distance) [31–33], and symmetry of individual quantum dots [34,35], and their misalignment [36,37] can provide additional leverage for controlling the spectral properties of these nanostructures. Additionally, post-growth control of quantum dot molecules can be achieved by applying external fields, in particular electric field that is applied in the growth direction [38–43]. The application of an external field allows the basic studies of quantum dot molecule spectra, and it is also a useful tool for tailoring quantum dot molecules for achieving novel applications [44–46]. Therefore, herein, we study the properties of several nanowire quantum dot molecules, with a high degree of alloying and resulting alloy randomness, under the influence of an external vertical field, focusing on their excitonic fine structure.

The rest of this paper is organized as follows. After a short theoretical introduction in Sec. II, in Sec. III we discuss the electric-field single-particle and excitonic spectra for two different quantum dot molecules formed by two quantum dots of different heights. In Sec. IV, we study the electric-field spectra for six random realizations of a quantum dot molecule, built from two quantum dots of nominally identical dimensions. Finally in Sec. V we summarize the paper.

II. SYSTEMS AND METHODS

We first determine the atomic positions that minimize the total elastic energy by using the valence force-field method proposed by Keating [47,48] and by minimizing the strain energy obtained using the conjugate gradient method [33,49]. Next, for strain-relaxed atomic positions, the single-particle

---

*mswider@fizyka.umk.pl
†mzielin@fizyka.umk.pl

spectra of electrons and holes are obtained using the empirical $sp^3d^5s^*$ tight-binding method (TB), which accounts for d-orbitals and spin-orbit interaction [50–53]. The tight-binding calculation is effectively performed on a smaller domain than the valence force-field calculation [54,55], with sufficient dimensions for obtaining electron and hole spectra with submillielectronvolt accuracy [54,55]. Nonetheless, the computational box contains approximately 1 million atoms. The details regarding the $sp^3d^5s^*$ tight-binding calculations for various nanostructures have been thoroughly discussed in our previous papers [33,52,53,56]. Since the atomistic theory of piezoelectricity for alloyed systems is still an active field of research [57], and due to the small ($\approx 0.6\%$) lattice mismatch between alloyed $InAs_{0.2}P_{0.8}$ quantum dots and the surrounding InP nanowire (five times smaller than for unalloyed InAs/InP system), we neglect the piezoelectric effects in the present calculation, following similar arguments by Gong *et al.* [58], who ignore piezoelectricity in the empirical pseudopotential work on InAs/InP quantum dots. A static vertical electric field is included in the tight-binding calculation through a potential-energy shift of the orbital energies [28,59]. Finally, the excitonic spectra [60] are calculated using the configuration interaction method (CI) described in detail in Ref. [56]. More details regarding the Coulomb matrix element computation for tight-binding wave functions can be found in Refs. [61,62] as well as in our recent studies [63,64]. In our numerical tests, we found that the perturbative approach [26,65] may fail to accurately describe the excitonic fine structure for larger fields. Therefore, the TB Hamiltonian (and the following CI problem) needs to be solved for each field value separately, thus constituting a formidable computational challenge with a total of over 400 combined TB/CI calculations.

To study the effects of alloy randomness, we focus on a uniform composition profile, rather than on the effects of spatial changes in the overall composition [66–68]. We account for intermixing by considering 80% admixture of barrier material in the dot region, i.e., an $InAs_{0.2}P_{0.8}$ quantum dot in the InP nanowire surrounding. To model alloying, with random alloy fluctuations, for each anion site in quantum dot regions, a random number (uniformly distributed within the 0–1 range) is generated, based on which an arsenic atom is replaced with a phosphorous atom with a probability of 0.8. Thus, this approach generates microscopic configurations that differ significantly in terms of the atomic arrangement while maintaining an average phosphorus content of 80%.

Finally, we emphasize that due to spin-orbit interaction, and low overall symmetry, due to underlying lattice with alloying, the spin is no longer a good quantum number, and thus the notion of a quasispin [69] should rather be used instead. Nonetheless, eigenstates of the tight-binding Hamiltonian are doubly degenerate to due to time-reversal-symmetry [70], and many authors continue to refer to electron and hole "spin" configurations [71] when discussing the bright exciton splitting in quantum dots.

III. DOUBLE QUANTUM DOTS WITH DIFFERENT HEIGHTS

First, we consider a quantum dot molecule formed by two quantum dots of substantially different heights: $h_{lo} = 7.7$ and
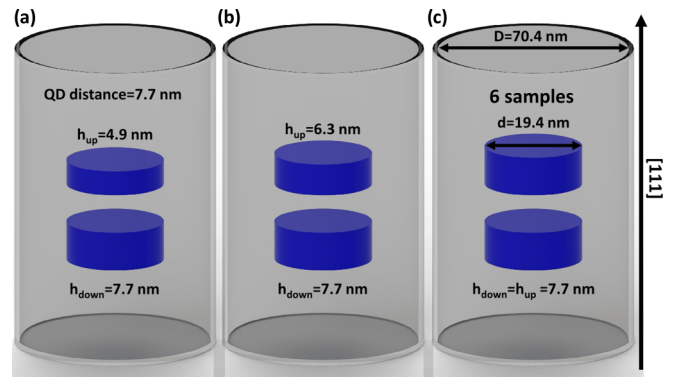

FIG. 1. Schematics of systems under consideration: (a),(b) alloyed $InAs_{0.2}P_{0.8}$ nanowire quantum dot molecules built from quantum dots of different heights and (c) with the same height but with six randomly generated samples (realizations) corresponding to the same average composition and different (random) atomic arrangements.

$h_{up} = 4.9$ nm [Fig. 1(a)]. The spacing between the top of the lower quantum dot and the bottom of the upper quantum dot is 7.7 nm (same as the height of the lower quantum dot); however, the diameters of both dots are equal to 19.4 nm. Such relatively large quantum dot heights are not only consistent with those obtained experimentally [12,17] but are also necessary to effectively confine the charge carriers (in particular, electrons) in very shallow confinement provided in a quantum dot with 80% barrier material (phosphorous) contribution.

Figure 2 shows the evolution of single-particle states as a function of the electric field for this system, and Fig. 3 and Fig. 4 show the corresponding probability density plots for several field values for electrons and holes, respectively. As apparent from single-particle spectra, the two lowest electron states form a pair of strongly coupled, molecular orbitals, with an anticrossing at approximately 100 kV/cm, where the formation of e_1 bonding and e_2 antibonding orbitals is particularly clear. The two lowest electron states remain significantly coupled in a broad range of considered field values, with the exception of negative fields, where they appear to separate into
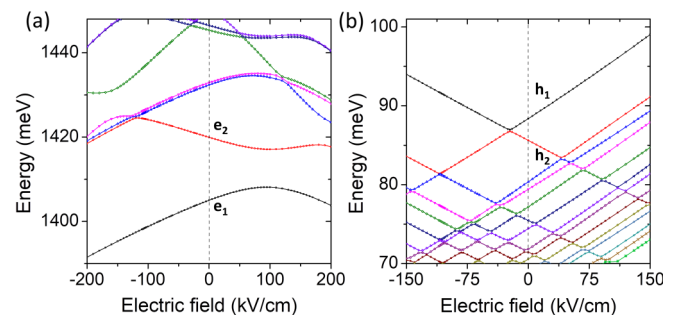

FIG. 2. Single-particle (a) electron and (b) hole spectra of the alloyed $InAs_{0.2}P_{0.8}$ nanowire quantum dot molecule formed from two quantum dots of substantially different heights ($h_{lo} = 7.7$ and $h_{up} = 4.9$ nm) as a function of the external electric field. Vertical dashed black lines are guides to the eye for zero-field cases. e_1 and e_2 indicate the ground-electron and first excited states, respectively, and h_1 and h_2 are used for the hole states. Note the reverse ordering of single-particle energies of hole states, as compared to electron states.
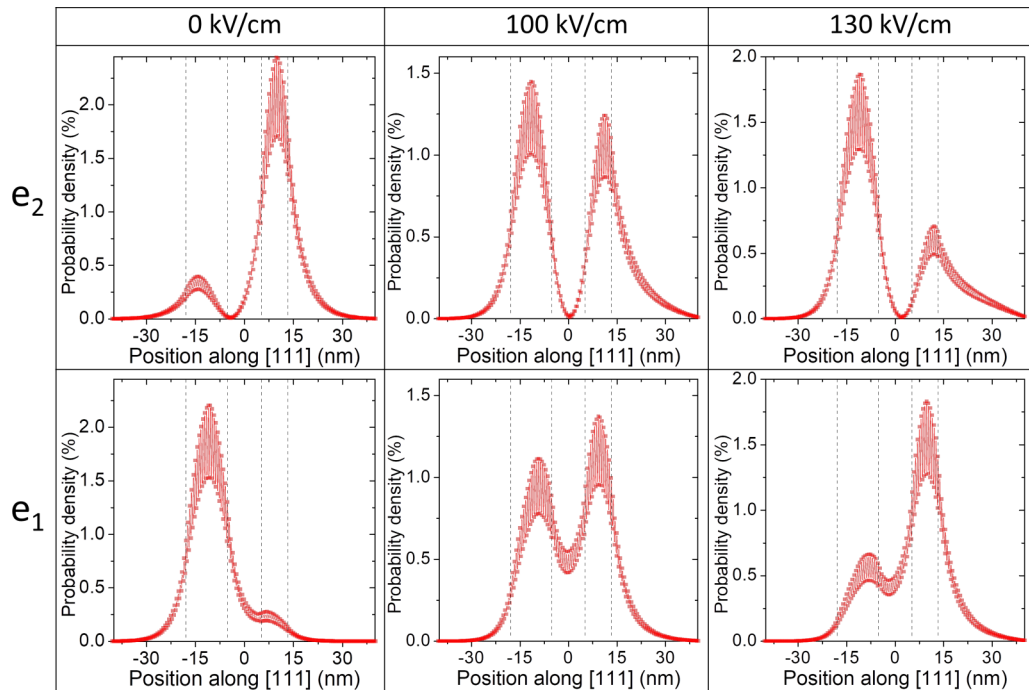
FIG. 3. Single-particle ground-electron (e_1) and excited-state (e_2) probability densities (integrated over the lateral plane) for a nanowire quantum dot molecule formed by two alloyed $InAs_{0.2}P_{0.8}$ quantum dots of significantly different heights ($h_{lo} = 7.7$ and $h_{up} = 4.9$ nm), for several values of the external electric field and as a function of position along the (vertical) growth [111] axis. Thin, vertical dashed lines indicate the positions of individual quantum dots. A strong oscillatory character is observed due to the presence of subsequent anion/cation monolayers. For a field of 100 kV/cm, a pair of apparent bonding and antibonding quasimolecular orbitals is formed and substantial tails at neighboring dots are present at other field values.
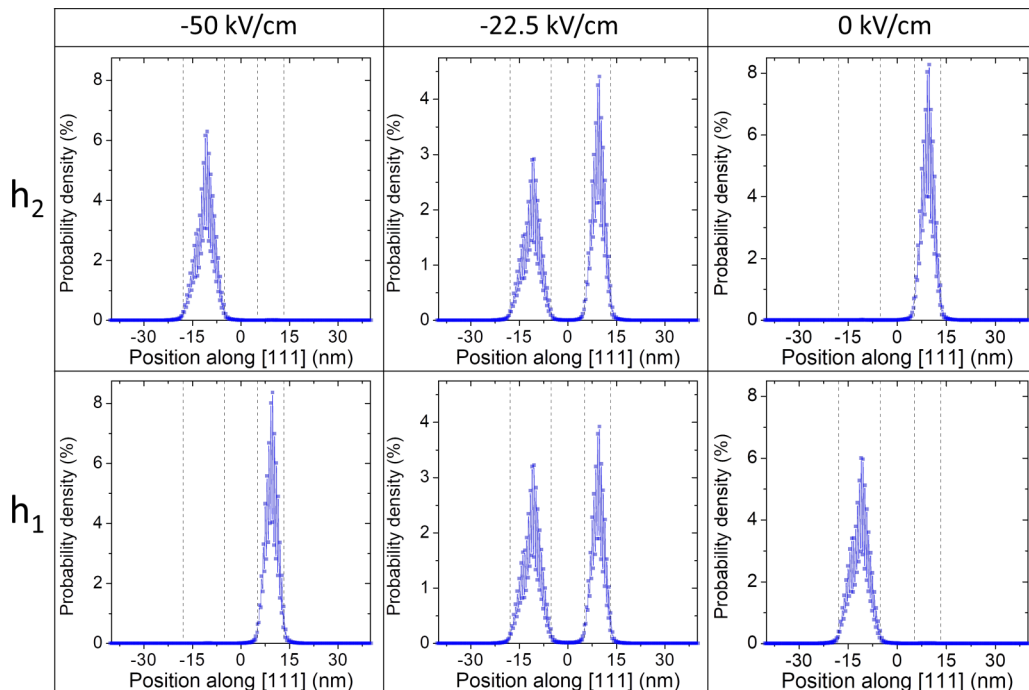

FIG. 4. Single-particle ground-hole (h_1) and excited-state (h_2) probability densities (integrated over the lateral plane) for a nanowire quantum dot molecule formed by two alloyed $InAs_{0.2}P_{0.8}$ quantum dots of significantly different heights ($h_{lo} = 7.7$ and $h_{up} = 4.9$ nm), for several values of the external electric field and as a function of position along the (vertical) growth [111] axis. Thin, vertical dashed lines indicate positions of individual quantum dots. A strong oscillatory character is observed due to the presence of subsequent anion/cation monolayers. Note again that much stronger confinement than that in the case of electron states is achieved. At a field of −22.5 kV/cm, a pair of bonding and quasimolecular orbitals is formed, whereas the other field-value hole states are well localized in separate quantum dots.
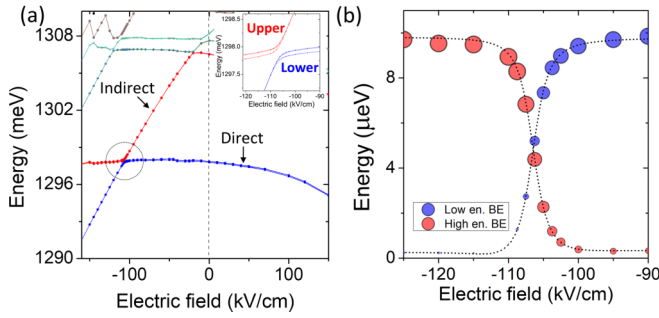
FIG. 5. (a) Exciton spectrum of a nanowire quantum dot molecule formed by two alloyed InAs$_{0.2}$P$_{0.8}$ quantum dots of significantly different heights ($h_{lo} = 7.7$ and $h_{up} = 4.9$ nm). The dashed circle indicates the region close to the excitonic anticrossing. The inset shows a magnification of the spectra close to the anticrossing. Energies for the high- and low-energy branch of the spectrum are plotted in dark gray (red) and light gray (blue), respectively. (b) Fine structure of the bright exciton spectrum near the anticrossing for the same nanowire quantum dot molecule. The dark gray (red) and light gray (blue) points correspond to the calculated fine structures of the high- and low-energy exciton branches, respectively. The energies are plotted relative to the central energy of each branch. Diameters of circles correspond to optical activity. The dashed lines are fitted to the atomistic results using the phenomenological model discussed in the text.

individual quantum dots. Such strong electron state coupling results from very shallow confinement in InAs$_{0.2}$P$_{0.8}$ alloyed systems and a pronounced leakage of electron probability density into the barrier material.

Contrarily, hole states tend to strongly occupy their constituent quantum dots with apparently much weaker coupling and the formation of molecularlike h_1 and h_2 orbitals only in the narrow vicinity of anticrossing at -22.5 kV/cm [Fig. 2(b) and Fig. 4]. Moreover, the spectrum of hole state resembles a sum of spectra of two individual quantum dot spectra with linearlike trends of their single-particle energies, evolving into opposite directions, and numerous crossings of excited yet confined hole states. In contrast, only six lowest electron states are confined in quantum dot molecules at zero field, with higher states being delocalized. Importantly, anticrossings for ground-electron- and hole states occur at notably different field values. In particular, hole anticrossing and formation of hole molecularlike orbitals occur at field values at which the ground-electron state is nearly fully localized in the lower dot.

The structure of single-particle states translates into excitonic spectra. In the case of quantum dot molecules formed by quantum dots of dissimilar sizes, these spectra can be interpreted [Fig. 5(a)] in terms of a direct exciton—formed by electrons and holes occupying the same, lower dot—and an indirect exciton—formed by the electron in the lower dot, yet the hole resides in the upper dot. The direct exciton with both charge carriers localized in the same dot is expected to show a rather weak energy evolution under the applied electric field. On the other hand, the indirect exciton with a strong built-in dipole moment due to the spatial electron-hole separation should be strongly affected by the field. Such trends are typical for double quantum dots of dissimilar sizes [26,42] resulting in pronounce direct-indirect exciton crossing resulting.

Matching random arrangements of atoms forming a quantum dot molecule, for different samples, with the resulting fine structure is a tremendous challenge. To overcome this problem, recently, for single quantum dots, we have augmented atomistic calculations with statistical analysis for 300 quantum dot random realizations [72] of the same quantum dot. Due to the prohibitive computational complexity of such an approach for the electric-field calculations, here we opt for a different path, and to gain a better understanding of atomistic results, we utilize a simple model of Sköld *et al.* [42] aiming to understand better the TB/CI results. In this approach, one defines a four-by-four Hamiltonian expanded in a basis of four electron-hole configurations: $|e_1h_1, H\rangle$, $|e_1h_1, V\rangle$, $|e_1h_2, H\rangle$, and $|e_1h_2, V\rangle$, where e_1 is the ground-electron state, and h_1 and h_2 are the ground- and first-excited-hole states, respectively. (H) and (V) stand for orthogonally polarized horizontal and vertical states (with different (quasi)spin alignments corresponding to H and V polarizations [42]). We note that dark states due to spin selection rules are omitted [71]. For a quantum dot molecule formed by quantum dots of dissimilar sizes $|e_1h_1, H\rangle$, $|e_1h_1, V\rangle$ correspond to the direct exciton configurations, whereas $|e_1h_2, H\rangle$ and $|e_1h_2, V\rangle$ describe the indirect exciton configurations. More details regarding this model can be found in Ref. [42].

We recently [28] extended an original model of Sköld *et al.* [42] to account for the nonlinearities of direct/indirect excitonic field evolution, as well as a strong dot-coupling regime, with $\mathbf{H} = \mathbf{H}_1 + \mathbf{H}_2$, where $\mathbf{H}_1$ describes the electric field dependence of the main excitonic spectral features and $\mathbf{H}_2$ is used for modeling the fine structural component of the exciton spectrum:

$$\mathbf{H} = \mathbf{H}_1 + \mathbf{H}_2 = \mathbf{I}E_X + \begin{bmatrix} p_D F + \beta F^2 & 0 & t & 0 \\ 0 & p_D F + \beta F^2 & 0 & t \\ t & 0 & E_h + p_I F + \beta_2 F^2 & 0 \\ 0 & t & 0 & E_h + p_I F + \beta_2 F^2 \end{bmatrix}$$

$$+ \begin{bmatrix} 0 & \delta_{DD} & 0 & \delta_{DI} \\ \delta_{DD} & S_D - \gamma_D F & \delta_{DI} & 0 \\ 0 & \delta_{DI} & 0 & \delta_{II} \\ \delta_{DI} & 0 & \delta_{II} & S_I - \gamma_I F \end{bmatrix}, \tag{1}$$

where I is the identity matrix, E_X is the energy of a neutral exciton confined in the larger quantum dot, E_h is the energy

required to move the hole from the larger quantum dot to the smaller quantum dot at zero field, t describes the hole-state

tunnel coupling strength, p_D and p_I are the dipole moments of direct and indirect excitons, respectively, β and β_2 are their corresponding polarizabilities, and F is the electric field. In the exchange part ($\mathbf{H}_2$) of the Hamiltonian, δ_{DD} and S_D describe the direct-exciton fine-structure splitting, where S_D is part of the bright-exciton splitting that can be tuned to zero by the electric field owing to the $-\gamma_D F$ term [42,73]. Thus, S_D reflects the difference in the permanent dipole moments between the two bright states of the direct exciton. δ_{II}, S_I, and $-\gamma_I$ are used for indirect excitons. The fine-structure coupling between the direct and indirect states is introduced by the δ_{DI} term (which is typically very small). Importantly, we treat E_X, δ_{DD}, and all other coefficients in $\mathbf{H}$ as fitting parameters, while fitting the atomistic results as a function of F and close to the excitonic anticrossing.

Figure 5(b) shows the bright-exciton splitting evolution of direct/indirect excitons near anticrossing, with dashed lines indicating an excellent fit to the atomistic results. The behavior shown in Fig. 5(b) is typical for a quantum dot molecule formed by two quantum dots of substantially different sizes, with a "dark" indirect exciton of nearly vanishing fine-structure splitting due to electron-hole separation, and a "bright" direct exciton that is optically active due to the electrons and holes residing in the same dot and exhibits non-negligible fine-structure splitting. Characteristically, at the anticrossing, the direct and indirect excitons "exchange" or "swap" their properties, where the higher-energy branch gains optical activity (and nonzero bright-exciton splitting), whereas the lowest-energy branch loses its optical activity and becomes "dark" with nearly vanishing fine-structure splitting. The notion of "dark" exciton must be used here extremely carefully as, apart from the reduced optical activity to perform electron-hole separation, there is a notion of bright and dark excitons due to the relative orientation of electron and hole spins. Therefore, at the anticrossing, there are four (two bright and two dark) direct exciton states crossing with four indirect exciton states, as shown in the inset of Fig. 5(a), although because of scale, the inset cannot show spectral details (or fine-structure splitting). Nonetheless, the inset clearly demonstrates the presence of exchange splitting between the lower (dark) and upper (bright) exciton states of the direct exciton on the order of 70 μeV, and this exchange splitting for the indirect states (nearly) vanishes away from the crossing.

In summary, quantum dot molecules formed by nanowire quantum dots of substantially distinct heights have excitonic spectra similar to those of double self-assembled quantum dots [42] or C_{2v} nanowire quantum dot molecules [28]. Nonetheless, the case of substantially distinct heights forms a necessary starting point for discussion in the following part of the paper.

Thus, it is instructive to further consider a case in which this height difference is less substantial, namely a quantum dot molecule formed by two quantum dots of comparable yet different heights: $h_{lo} = 7.7$ and $h_{up} = 6.3$ nm [Fig. 1(b)]. The single-particle spectra of this system show an electric-field evolution comparable to that of a previously studied case (Fig. 6); however, it has notable differences with respect to the electron probability densities (Fig. 7), where we observe a more pronounced coupling of the electron states. Therefore, larger tails are observed in the other dot even further from the
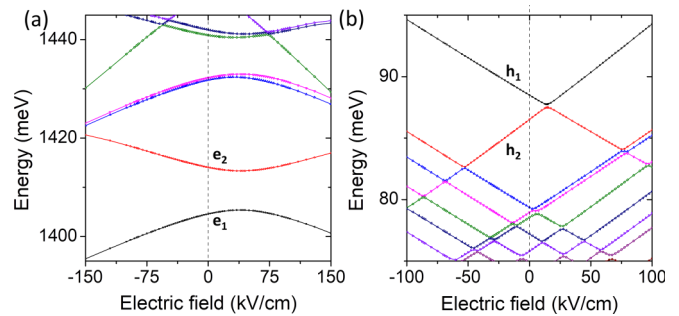

FIG. 6. Single-particle (a) electron and (b) hole spectra of the alloyed $InAs_{0.2}P_{0.8}$ nanowire quantum dot molecule formed from two quantum dots of slightly different heights ($h_{lo} = 7.7$ and $h_{up} = 6.3$ nm), as a function of the external electric field. Vertical dashed black lines are guides to the eye for zero-field cases. e_1 and e_2 are the ground-electron and first-excited states, and h_1 and h_2 indicate the hole states, respectively. Note the reverse ordering of hole states.

anticrossing, the anticrossing for the states of electrons e_1 and e_2 occurs at smaller field values (of 40 kV/cm), and finally, many similar maxima of probability densities are achieved for both dots for bonding and antibonding states. All these effects are attributed to the smaller difference in quantum dot heights, compared with the previous case.

Similarly, the hole spectra resemble those considered in the previous case, with the exception of hole anticrossing occurring at the positive field of 15 kV/cm, as shown in Fig. 6(b). A further inspection of the corresponding charge densities shown in Fig. 8 reveals another striking difference: A ground-hole state h_1 is not localized in the lower, larger quantum dot but in the upper quantum dot. This behavior is attributed to alloy randomness, which overcomes the confinement difference caused by the difference in the heights of the quantum dots and allows the ground-hole state to be localized in the upper dot. In other words, the confinement profile results from the combined effect of the spatial dimensions and composition (alloying). Because we do not perform calculations in the virtual-crystal approximation, we allow random fluctuations which may overcome the differences resulting from the different heights of the quantum dots.

As a result of these "inverted" hole-state spectra, hole anticrossing occurs for a positive value (15 kV/cm) and is relatively close to the electron anticrossing (at 40 kV/cm). Therefore, in a range of strong hole state coupling, electrons remain largely delocalized over both dots. In other words, the electron has comparable probability densities in both dots at field values at which the hole tunnels between the two dots. In excitonic language, this will blur the traditional meaning of direct/indirect excitons and affect excitonic field evolution, as shown in Fig. 9, where both the lower and upper excitonic branches exhibit pronounced nonlinear behavior. The peculiarity of this system is also pronounced close to the anticrossing, where it is apparent [inset in Fig. 9(a)] that both the upper and lower branches have nonzero exchange splitting (dark/bright exciton splitting), which is a signature of electron delocalization over both quantum dots. This is further observed on quite a surprising excitonic fine-structure evolution at the anticrossing level, as shown in Fig. 9(b). In this figure,
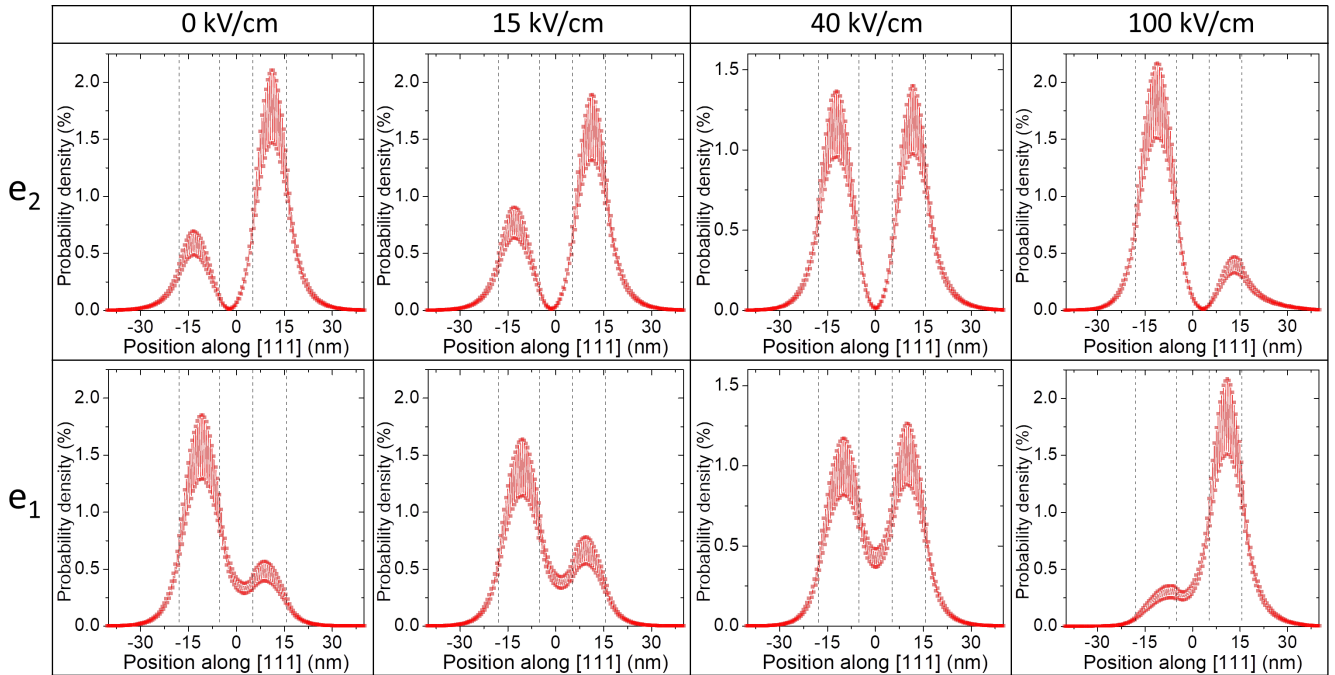
FIG. 7. Single-particle ground-electron (e_1) and excited-state (e_2) probability densities (integrated over the lateral plane) for a nanowire quantum dot molecule formed by two alloyed $InAs_{0.2}P_{0.8}$ quantum dots of slightly different heights ($h_{lo} = 7.7$ and $h_{up} = 6.3$ nm), for several values of the external electric field and as a function of position along the (vertical) growth [111] axis. Thin, vertical dashed lines indicate positions of individual quantum dots. Strong oscillatory characteristic is observed owing to the presence of subsequent anion/cation monolayers. At a field of 40 kV/cm, a pair of apparent bonding and antibonding quasimolecular orbitals is formed, with even larger tails observed at neighboring dots than those in the case of dissimilar quantum dot heights.
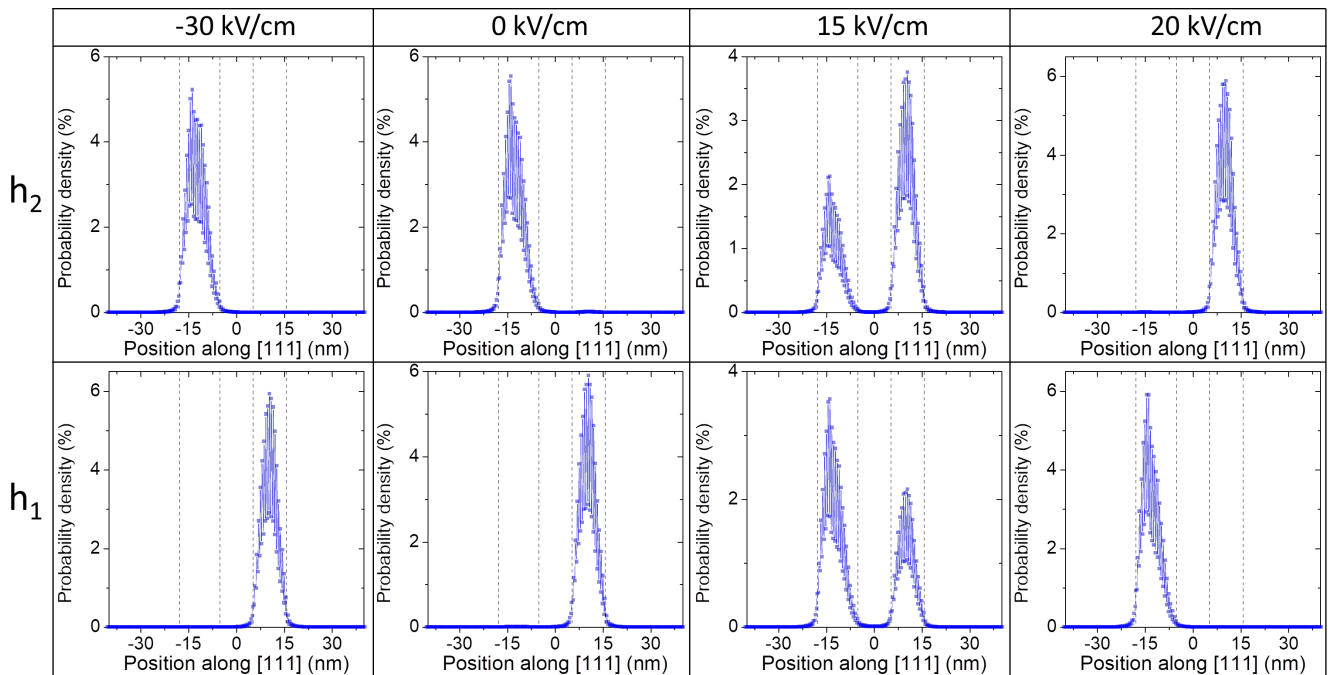

FIG. 8. Single-particle ground-hole (h_1) and excited-state (h_2) probability densities (integrated over the lateral plane) for a nanowire quantum dot molecule formed by two alloyed $InAs_{0.2}P_{0.8}$ quantum dots of slightly different heights ($h_{lo} = 7.7$ and $h_{up} = 6.3$ nm), for several values of the external electric field, and as a function of position along the (vertical) growth [111] axis. Thin, vertical dashed lines indicate positions of individual quantum dots. Strong oscillatory character is observed owing to the presence of subsequent anion/cation monolayers. Note that much stronger confinement than that for electron states is achieved. At a field of 15 kV/cm, a pair of bonding and quasimolecular orbitals is formed, whereas, for other field values, the hole states remain well localized in separate quantum dots.
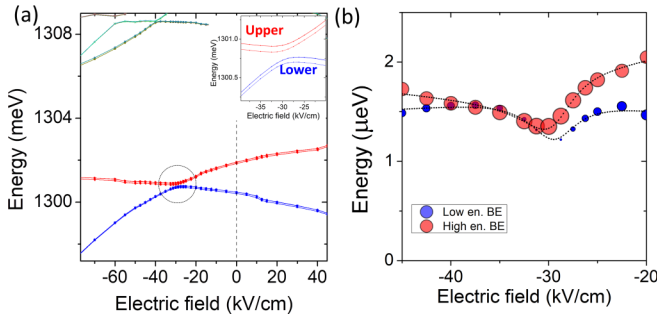
FIG. 9. (a) Exciton spectrum of a nanowire quantum dot molecule formed by two alloyed $InAs_{0.2}P_{0.8}$ quantum dots of slightly different heights ($h_{lo} = 7.7$ and $h_{up} = 6.3$ nm). The dashed circle indicates the region close to the excitonic anticrossing. The inset shows magnified spectra close to the anticrossing. Energies for the high- and low-energy branch of the spectrum are plotted in dark gray (red) and light gray (blue), respectively. (b) Fine structure of the bright-exciton spectrum near the anticrossing for the same nanowire quantum dot molecule. The dark gray (red) and light gray (blue) points correspond to the calculated fine structures of the high- and low-energy exciton branches, respectively. The energies are plotted relative to the central energy of each branch. Diameters of circles correspond to optical activity. Dashed lines are fitted to the atomistic results by using the phenomenological model discussed in the text.

both the lower and upper branches have comparable fine structure splitting; however, the upper branch (nominally "indirect" exciton) has a larger splitting magnitude and nonzero optical activity away from the crossing (in particular, at zero field). At the anticrossing of -30 kV/cm, the lower excitonic branch loses its optical activity, whereas the other branch has it increased; however, this branch does not have vanishing optical activities away from the anticrossing, including the zero field [not shown in Fig. 9(b)]. Furthermore, there is no substantial exchange/swap of fine-structure splitting between the excitonic branches, and only a small dip is observed close to the crossing. In fact, both excitonic branches have rather small fine-structure splitting, reaching at most 2 μeV [Fig. 9(b)]. This is a striking difference with respect to a previous case; however, in alloyed nanowire quantum dots and quantum dot molecules, the fine-structure splitting strongly varies between the dots because of the alloy randomness. Therefore, the striking difference between the fine structure spectra of $h_{lo} = 7.7/h_{up} = 4.9$ nm versus $h_{lo} = 7.7/h_{up} = 6.3$ nm may not be related to the h_{up} difference but sample dependence due to alloy randomness.

IV. DOUBLE QUANTUM DOTS WITH IDENTICAL HEIGHTS: RANDOM SAMPLES

To determine how the excitonic electric-field spectra vary depending on alloy randomness, we consider six random samples (random realizations) for a quantum dot molecule formed by two $InAs_{0.2}P_{0.8}$ quantum dots of identical heights [Fig. 1(c)]. We emphasize that the condition of identical heights is not essential from neither theory or experiment point of view. Those identical height were chosen here simply to study the net effect of alloying rather than a combined effect of alloying and height fluctuations. Since we consider

quantum dots similar to those single dots obtained experimentally, they have rather large heights (7.7 nm) and strong (80%) intermixing with a barrier material, leading therefore to rather broad (in the growth direction) and shallow confining potentials. The vertical confinement is thus weak and variations of height lead to a rather small [25] changes in excitonic energy, whereas energies due to alloying can be substantial and dominate over fluctuations of quantum dot heights.

We start with single-particle ground-electron and hole state probability densities at the zero field for each random sample, as shown in Fig. 10. In all considered cases, the electron state shows a very similar probability distribution with a notably larger probability in the lower dot. Because this feature is shared by all samples, it is not related to alloy randomness. Moreover, as this is observed for a quantum dot molecule formed by dots of identical heights, this effect is related to the lack of inversion symmetry in the growth direction for the [111]-oriented systems [26], leading to an increased probability electron density in the bottom quantum dot. The lack of inversion symmetry is triggered by [111] oriented substrate and is mostly mediated by strain [26]. For unalloyed systems, the combination of disk shape and underlying [111] oriented nanowire symmetry leads to overall C_{3v} symmetry, and irreducible representations of the C_{3v} group does not contain the rotoinversion ('improper rotation') operation [74], which is characteristic for D_{2d} symmetry of an idealized, symmetric quantum well or quantum dot grown in the crystallographic [001] direction. Thus the C_{3v} disk shape quantum dot states (or quantum dot molecule states) lacking this symmetry operation will in principle not have the inversion symmetry in the growth direction. For alloyed systems the strain and strain-related anisotropy is strongly reduced, nonetheless, the electron ground state still tends to localize preferably in the lower dot, yet with a significant contribution in the upper dot as well. In contrast, the ground-hole localization is dominated by alloy randomness, with the ground-hole state localized predominantly either in the bottom quantum dot (samples 1 and 4) or the upper quantum dot (samples 2, 5, and 6) or even forming a delocalized quasimolecular orbital at zero field (sample 3).

As mentioned earlier to model alloyed $InAs_{0.2}P_{0.8}$ quantum dots, with random alloy fluctuations, for each anion site in quantum dot regions, a random number generated, based on which an arsenic atom is replaced with a phosphorous atom with a probability of 0.8. Thus, this approach generates microscopic configurations that differ significantly in terms of the atomic arrangement while maintaining an average arsenic content of 20%. A careful inspection reveals that such a procedure may result in random realizations that differ from the average composition between quantum dots within a range of approximately ± 0.5%, as shown in Table I. In general, for samples 1, 2, 4, and 5, a larger amount of arsenic in a given dot is correlated with the preferential localization of the ground-hole state in that dot (Fig. 10). For sample 6, one might expect the ground-hole state to be localized in the bottom dot instead, and for sample 3 as well, one would expect localization in the bottom dot instead of delocalized quasimolecular orbital formation with a maximum in the upper dot. As we consider relatively fewer samples and focus on electric-field dependencies, we cannot form any strong statistical statements [72].
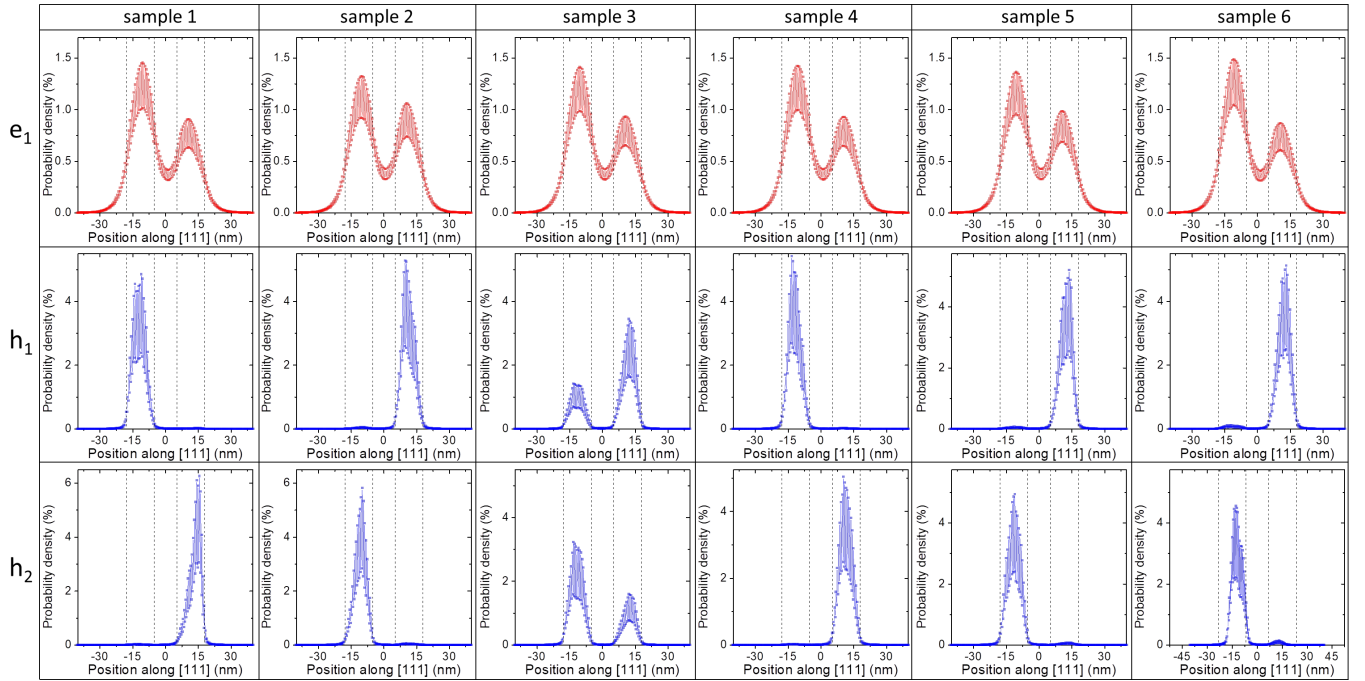
FIG. 10. Single-particle ground-electron (e_1, upper row) and hole (h_1, middle row and h_2, lower row) probability densities for a nanowire quantum dot molecule formed by two alloyed $InAs_{0.2}P_{0.8}$ quantum dots of identical heights ($h_{lo} = h_{up} = 7.7$), as well as for six random realizations (samples) and as a function of position along the (vertical) growth [111] axis. Thin, vertical dashed lines indicate positions of individual quantum dots.

However, hole localization is not only related to fluctuations in the average composition in each dot but also to mere alloy randomness (different random arrangements in the crystal lattice of the same number of atoms). Moreover, other effects that go beyond this study, such as a nonuniform composition profile, can affect such statistics.

The stability of the ground-electron-state charge distribution is reflected in the single-particle energy at zero field, as shown in Table II, which varies only within the 1 meV range (i.e., from 1403 to 1403.9 meV). The changes in the ground-hole-state h_1 single-particle energies are more pronounced (from 84.9 to 88.7 meV), consistent with the larger hole states' susceptibility to alloying [26], and the energetic variations of h_2 are equally substantial (from 84.6 to 87.6 meV). Large variations in h_1 and h_2 energies due to alloying lead to the reordering of the h_1 ground-state localization, as shown earlier in Fig. 10, where h_1 is typically localized in either of the dots,

TABLE I. Arsenic content in lower (QD1) and upper (QD2) quantum dots for each of the six random samples (realizations) for a nanowire quantum dot molecule formed by two alloyed $InAs_{0.2}P_{0.8}$ quantum dots of identical heights ($h_{lo} = h_{up} = 7.7$).

Sample	QD1 (%)	QD2 (%)
1	20.08	19.88
2	20.13	20.32
3	20.27	19.94
4	19.95	19.81
5	19.91	19.92
6	20.19	19.94

whereas h_2 is localized correspondingly in the opposite dot. This is reflected in the $h_2 - h_1$ energy difference shown in Table II. Only for sample 3, this energy difference is small, leading to the formation of a quasimolecular orbital. However, for samples 1, 2, and 4, this energy difference can be substantially larger than 1 meV. Because we are dealing with quantum dots of substantial vertical height and an admixture of barrier material quantum dots, both leading to relatively weak confinement in the vertical direction, alloy randomness may compete with a difference in quantum dot height and a reversal of hole confinement is apparently possible for double quantum dots of identical heights and also for double quantum dots of different yet comparable heights, as shown earlier for the $h_{lo} = 7.7 / h_{up} = 6.3$ nm system.

We also see that the ground electron e_1 state spatial localization varies very weakly between samples, with e_1 localized predominately in the dots area, though with pronounced tails in the barrier. In terms of numbers, this corresponds to 68.1% to 68.7% contribution localized within both quantum dots volumes. The substantial tails in the InP barrier thus vary from 31.3% to 31.9% correspondingly. The h_1—as well as h_2—hole spatial localization is much stronger with 96.3% to 96.9% (3.1% to 3.7%) in the dot (barrier) area, and again it only weakly changes on a system-to-system basis.

Finally, we also checked that for h_1 and h_2 states spin mixing [35,36] is actually rather weak, with 95% to 97% of one spin component (and thus 3% to 5% admixture of the other spin component respectively). Moreover, the spin mixing does not vary considerably between different random samples, nor it is strongly affected by the electric field. The degree of spin mixing for the ground electron state is even smaller, actually being very minimal, with well over 99% content of a dominant

TABLE II. Single-particle electron (e_1) and hole ($h1$, $h2$) energies, excitonic ground-state energy (E_X), and electron-hole Coulomb integrals calculated for the electrons and holes in their respective ground states J_{e1h1}, the electron in the ground state, and hole in the first excited state J_{e1h2}. Results are shown for each of the six random samples (realizations) and for a nanowire quantum dot molecule formed by two alloyed $InAs_{0.2}P_{0.8}$ quantum dots of identical heights ($h_{lo} = h_{up} = 7.7$). For convenience, $h_2 - h_1$ and J_{e1h1}-J_{e1h2} are also presented. All units are meVs.

Sample	e_1	h_1	h_2	$h_2 - h_1$	E_X	J_{e1h1}	J_{e1h2}	$J_{e1h1} - J_{e1h2}$
1	1403.4	87.9	86.2	1.70	1298.3	14.5	11.7	2.77
2	1403.0	88.7	87.6	1.11	1298.1	12.9	13.9	−1.08
3	1403.8	84.9	84.6	0.26	1302.6	12.6	13.3	−0.72
4	1403.9	86.5	84.8	1.69	1300.7	13.8	12.1	1.75
5	1403.9	86.6	85.7	0.89	1301.3	12.4	14.0	−1.61
6	1403.4	87.1	86.5	0.65	1299.9	12.0	14.5	−2.51

spin component. We note that eigenstates of the tight-binding Hamiltonian are Kramers doublets [70]. Thus, to calculate the degree of spin mixing, within each doublet we diagonalize numerically the spin projection operator of the free electron $\hat{S}_z$ [75,76]. $\hat{S}_z$ eigenvector is also an eigenstate of the tight-binding Hamiltonian, for which we can determine (sum up) spin-up and spin-down contributions. We will further study the role of spin mixing in alloyed quantum dot molecules in our future work.

Ground hole-state localization in either lower or upper quantum dot must be reflected in the excitonic spectra. In particular, the ground-exciton-state energy E_X, dominated by configurations involving e_1 and h_1 states, is given as follows [58,77,78]: $E_X = e_1 - h_1 - J_{e1h1} - \Delta_{corr}$, where e_1 and h_1 are the particle electron and hole energies, respectively, J_{e1h1} is the electron-hole Coulomb attraction calculated for the electrons and holes in their respective ground states, and Δ_{corr} is the correction resulting from the exchange and correlation effects. As shown in Table II, at zero field, such a scenario occurs for cases where the hole is localized predominately in the lower dot (samples 1 and 4) owing to the larger electron localization in the lower dot, the electron-hole attraction between e_1 and h_1 has a larger magnitude than that between e_1 and h_2, and the ground excitonic state is built predominantly from excitonic configurations involving e_1 and h_1. This is exactly the case for samples 1 and 4, where configurations involving e_1-h_1 states (with four different quasispin configurations) contribute to over 80% of the lowest four exciton states, whereas those involving e_1 and h_2 contribute to building over 70% of the next four (excited) excitonic states. Therefore, these cases correspond to a typical picture in which the lowest excitonic states are built predominantly from configurations involving the ground-hole state localized in the lower dot.

In contrast, for the ground-hole state localized in the upper dot, when the difference between J_{e1h1} and J_{e1h2} overcomes single-particle spacing $h_2 - h_1$, such as that in sample 6, these images will be reversed with e_1-h_2 contributions dominating (79%) the ground exciton state and the lowest four excitonic states, whereas the next four excited states will be predominately (up to 70%) constituted by e_1-h_1 configurations (again, with different spin alignments). Thus, for sample 6, the lowest four excitonic states are built predominately from the configurations involving the first-excited ground-hole state, although localized in the lower dot.

On the other hand, for samples 2 and 5, the difference J_{e1h1}-J_{e1h2} is apparently unable to overcome single-particle

$h_2 - h_1$ energy spacing, with ground exciton states having 75% and 63% contributions from e_1-h_1 configurations for samples 2 and 5, respectively. Thus, in these two cases (samples 2 and 5), the lowest four excitonic states are built from configurations involving the ground hole h_1, which is localized in the upper dot. Next, sample 3, which has the smallest $h_2 - h_1$ difference and for which h_1 is strongly delocalized over both dots (Fig. 10), forms an intermediate, strongly mixed case with 42% contributions involving e_1-h_2 states and 23% contributions from configurations involving e_1-h_1 states.

Finally, addressing electron contributions to many-body states, for all samples considered here, there are pronounced contributions from configurations involving the first excited electron state e_2. In particular, there are 13% to 24% (average of 17%) contributions involving e_2 to lowest four excitonic states (constituting "direct" exciton manifold), and—typically somewhat larger—contributions from 12% to 31% (average of 23%) to next higher four excitonic states (those constituting "indirect" exciton manifold).

Therefore, all six random realizations, despite having very similar excitonic energies (Table II), have substantially different excitonic configurations at zero field, with competition between single-particle energy differences and Coulomb interactions and notable many-body mixing involving both lowest two electrons and lowest two hole states. Therefore, one can expect nontrivial electric-field excitonic evolution and optical spectra, as will be shown later.

Single-particle electric-field energy spectra for quantum dot molecules built from quantum dots of nominally identical height, for six random samples, qualitatively resemble those of previously considered cases of dissimilar heights, and as such, are shown in the Appendix for completeness. However, for the six random samples, as discussed earlier, the hole ground may be located in either quantum dot (Fig. 10); thus, the corresponding first excited hole state (h_2) will be localized in the opposite dot. Therefore, a single-particle hole anticrossing will occur at different field values (see the Appendix), and the excitonic spectra will be altered correspondingly.

A. Bright-exciton splitting and the simple model

As shown in Fig. 11(a), for the six random samples considered here, it is difficult to maintain the notion of direct/indirect excitons, with different slopes of lower/upper energy branches, and their strongly nonlinear characteristic. Nonetheless, besides quantitative differences, the overall ex-
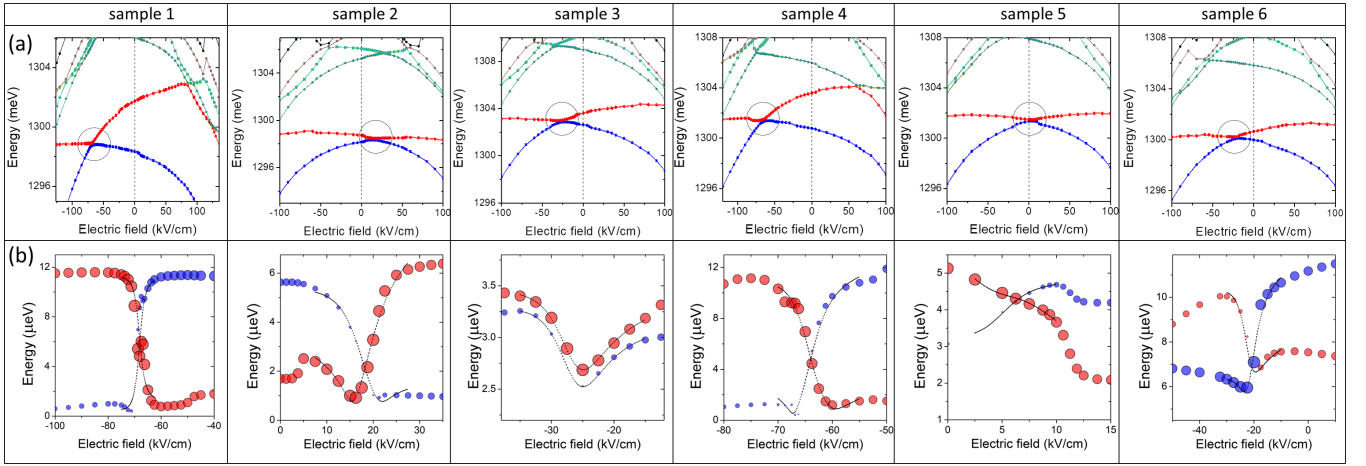
FIG. 11. (Upper row) Excitonic spectrum of a nanowire quantum dot molecule formed by two alloyed InAs$_{0.2}$P$_{0.8}$ quantum dots with identical heights ($h_{lo} = h_{up} = 7.7$) and for six random realizations (samples). Dashed circles indicate the region close to the excitonic anticrossings. (Lower row) Corresponding fine structure of bright-exciton spectra near the anticrossings. The dark gray (red) and light gray (blue) points correspond to the calculated fine structures of the high-and low-energy exciton branches, respectively. The energies are plotted relative to the central energy of each branch. The diameters of the circles correspond to the optical activity. Dashed lines are fitted to the atomistic results obtained using the phenomenological model discussed in the text.

citonic spectra are qualitatively similar to each other, although the lower and upper branches have different tilts and their anticrossings occur for both negative and positive field values depending on the case. In contrast, the excitonic fine-structure field evolution varies tremendously from one quantum dot molecule realization to another, as shown in Fig. 11(b). For samples 1, 2, and 4, the overall picture is somewhat similar to the case of a quantum dot molecule formed by two quantum dots of distinct dimensions. Yet, for sample numbers 3, 5, and 6, this evolution is more complicated, with sample number 3 revealing some similarity to a single random realization studied earlier for the $h_{lo} = 7.7/h_{up} = 6.3$ nm system. To quantify these differences, we performed a series of fits to the model of Eq. (1), for each random sample, with the results of the fits related to the exchange part of the Hamiltonian (**H**$_2$) shown in Table III and other fitting parameters (related to **H**$_1$) shown in Table IV in the Appendix. Finally, we note, that the parameters introduced in Table III and Table IV have been obtained by fitting first the main features in the excitonic spectra, such as those presented in Fig. 11(a), i.e., that without accounting for the fine-structure splitting. This allows to establish parameters of the **H**$_1$ part of the Hamiltonian (such

as t or p_D etc.). Next, we fix H_1 parameters subset and fit the rest of the parameters (from H_2 part, such as S_D etc.) to match the fine-structure spectra evolution in the region close to the anticrossing. All calculations were performed using the nonlinear regression approach as implemented in *nlinfit* function of MATLAB [79] environment.

Although the notion of direct/indirect excitons is no longer valid for a system of identical heights, alloyed quantum dots, the model of Eq. (1) still fits the atomistic results well (dashed lines in the lower row of Fig. 11), at least near the anticrossing, whereas it typically fails far from the crossing. Contrary to the $h_{lo} = 7.7/h_{up} = 4.9$ nm system, an analysis of Eq. (1) parameters presented in Table III is complicated because all parameters are strongly affected by alloying and vary on a system-to-system basis. Nonetheless, by performing fits and analyzing different parameters, we found that the relative magnitudes of S_D and S_I are important. If the magnitude of S_D component is comparable to that of S_I, then an "atypical" behavior is observed, as observed for samples 3, 5, and 6. Contrarily, if the magnitude of S_D substantially differs from that of S_I, a more "typical" pattern of both branches swapping their fine structure splitting emerges. This pattern also ap-

TABLE III. Parameters of Hamiltonian **H**$_2$ obtained by fitting to atomistic results. δ and S values are given by μeV. γ values are given in $10^{-2} \times \mu$eV kV^{-1} cm.

QD molecule	S_D	S_I	δ_{DD}	δ_{II}	γ_D	γ_I	δ_{DI}
$h_{lo} = 7.7$ nm, $h_{up} = 4.9$ nm	7.90	-0.46	2.91	0.06	0.000	0.016	-0.15
$h_{lo} = 7.7$ nm, $h_{up} = 6.3$ nm	-1.19	-1.99	-0.31	0.77	-0.091	0.353	-0.12
$h_{lo} = h_{up} = 7.7$ nm; sample 1	11.48	-2.26	-0.24	-0.37	-0.016	0.34	0.96
sample 2	0.62	3.10	2.78	-0.72	1.86	0.64	-0.26
sample 3	2.20	3.11	1.20	-0.86	0.044	-0.10	-0.32
sample 4	15.25	10.69	5.13	-0.95	-1.60	-1.73	-0.85
sample 5	-6.23	7.68	1.43	2.63	-4.68	7.01	-0.29
sample 6	-7.43	7.46	2.02	4.75	0.70	-1.01	-0.26

TABLE IV. Parameters of H_1 obtained by fitting to atomistic results. The parameters t, E_h, and E_X are given in meV, p_D and p_I in $10^{-1} \times$ meV kV^{-1} cm, and β and β_2 are given as $10^{-4} \times$ meV kV^{-2} cm^2.

QD molecule	t	p_D	p_I	E_h	β	β_2	E_X
$h_{lo} = 7.7$ nm, $h_{up} = 4.9$ nm	−0.127	0.180	9.295	10.723	−0.136	−1.023	1298.266
$h_{lo} = 7.7$ nm, $h_{up} = 6.3$ nm	−0.092	−1.462	2.277	1.352	−0.853	−3.944	1300.484
$h_{lo} = h_{up} = 7.7$ nm; sample 1	−0.078	1.543	−6.414	−0.247	1.495	−9.642	1299.235
sample 2	0.077	0.856	−0.440	0.332	0.033	−3.537	1298.280
sample 3	−0.086	−1.096	1.168	0.742	−0.923	−2.968	1302.727
sample 4	−0.098	−6.277	9.878	6.816	−5.135	3.574	1299.533
sample 5	−0.067	0.582	0.198	0.028	5.021	−11.994	1301.434
sample 6	0.081	−0.694	1.949	0.681	0.015	−2.372	1300.040

plies to $h_{lo} = 7.7/h_{up} = 4.9$ nm and $h_{lo} = 7.7/h_{up} = 6.3$ nm systems. Note that S_D and S_I can have both negative and positive values, indicating a reversal of the fine-structure splitting between the lower and upper excitonic branches. While we retain direct and indirect indices, S_D should be interpreted as related to a lower excitonic branch before the anticrossing and not necessarily to the direct exciton, and S_I to be related to an upper excitonic branch and not necessarily an indirect exciton. Similarly, δs (parts of bright-exciton splitting that cannot be removed by alloying) with magnitudes varying from 0.24 to 5.13 μ eV, as well as γs, are also strongly affected by alloying. Finally, δ_{DI} typically plays a minor role.

Besides the phenomenological model, as a rule of thumb, at zero field, if the bright-exciton splitting of the lower branch ("direct") is larger than that of the higher branch (e.g., 5.6 vs 1.7 μeV for sample 2), then at the anticrossing, both branches tend to "swap" their fine-structure properties. In contrast, if at zero fields, the fine-structure splitting is comparable (sample 6) or even larger for the higher-energy exciton branch (e.g., sample 5), the bright-exciton evolution at the anticrossing is far from trivial. Another hint to predict such behavior originates from the analysis of $h_2 - h_1$, as shown earlier in Table II. Samples 1, 2, and 4 have substantially larger single-particle ground hole-first excited hole-state energy differences and reveal more traditional patterns (in particular, sample 1 with $h_2 - h_1 = 1.7$ meV), whereas samples 3, 5, and 6 with $h_2 - h_1$ smaller than 1 meV reveal more complicated bright-exciton splitting evolution (in particular, sample 3 with $h_2 - h_1$ as small as 0.26 meV).

B. Optical spectra

Despite the complicated patterns of bright-exciton splitting field evolution, all random samples share very similar behavior in the optical activity (circle sizes in the lower row of Fig. 11). This similarity is more apparent in Fig. 12, where the electric-field evolution of the lower and higher branches' optical activities is shown again, this time in the form of line plots. From a quantum dot molecule built from notably different heights ($h_{lo} = 7.7$ and $h_{up} = 4.9$ nm; a top-left corner in Fig. 12) and away from the anticrossing, there is a noticeable difference between the large optical activity of the lower-energy branch (direct exciton) and the low optical activity of the higher-energy branch (indirect exciton), with both branches apparently swapping their properties at the crossing.

This behavior substantially differs from that of a system built from identical-height quantum dots (six random samples) as well as for quantum dots of comparable heights ($h_{lo} = 7.7$ and $h_{up} = 6.3$ nm; top-right corner in Fig. 12). In these cases, at the anticrossing, the lower excitonic branch loses a pronounced fraction of its optical activity, whereas the higher-energy branch gains it. This mixing occurs most importantly at the anticrossing only, and further away from the anticrossing, both lower and higher excitonic branches exhibit comparable optical activities, with the higher-energy branch tending to have a stronger oscillator strength. In several cases (most importantly, samples 1, 2, and 4), the rebound of optical activity away from the anticrossing in Fig. 12 is assisted by a simultaneous reduction of the lower-branch bright-exciton splitting, which can still be tuned below 1 μeV and is a typical threshold for entanglement generation, while retaining significant optical activity.

C. Simplified analysis of optical spectra

To further study this effect, we utilized a toy model based on Eq. (1) which we describe in detail in the Appendix and which was used in Fig. 13(a). As shown in Fig. 13(a), a very simple approach reproduces a "standard" fine-structure splitting field evolution, with lower and higher branches "swapping" their properties at the crossing. A simple model thus reproduces the properties of quantum dots with identical heights (as in samples 1, 2, or 4) and double quantum dots of notably different heights (as in $h_{lo} = 7.7/h_{up} = 4.9$ nm). However, these two situations differ significantly in the ground-electron-state e_1 localization. Namely, for a quantum dot molecule formed by two quantum dots of substantially different heights (such as $h_{lo} = 7.7/h_{up} = 4.9$ nm), the ground-electron state is mostly pinned to a larger (lower) quantum dot at the excitonic anticrossing, whereas for the case of identical quantum dot heights (such as in samples 1, 2, and 4), it is delocalized over both dots. Moreover, the Hamiltonian in Eq. (1) is defined on the basis of $|e_1 h_1\rangle$ and $|e_1 h_2\rangle$ states—with different (quasi)spin alignments corresponding to H and V polarizations [42], and hence, on the basis of the following four states: $|e_1 h_1, H\rangle$, $|e_1 h_1, V\rangle$, $|e_1 h_2, H\rangle$, and $|e_1 h_2, V\rangle$. In the case of dissimilar heights, the quantum dot $|e_1 h_2, H/V\rangle$ is an indirect, "dark" state. However, for identical heights, e_1 is delocalized over both quantum dots; thus, both $|e_1 h_1, H/V\rangle$ and $|e_1 h_2, H/V\rangle$ are optically active and the notion of direct/indirect excitons is lost. Because the exci-
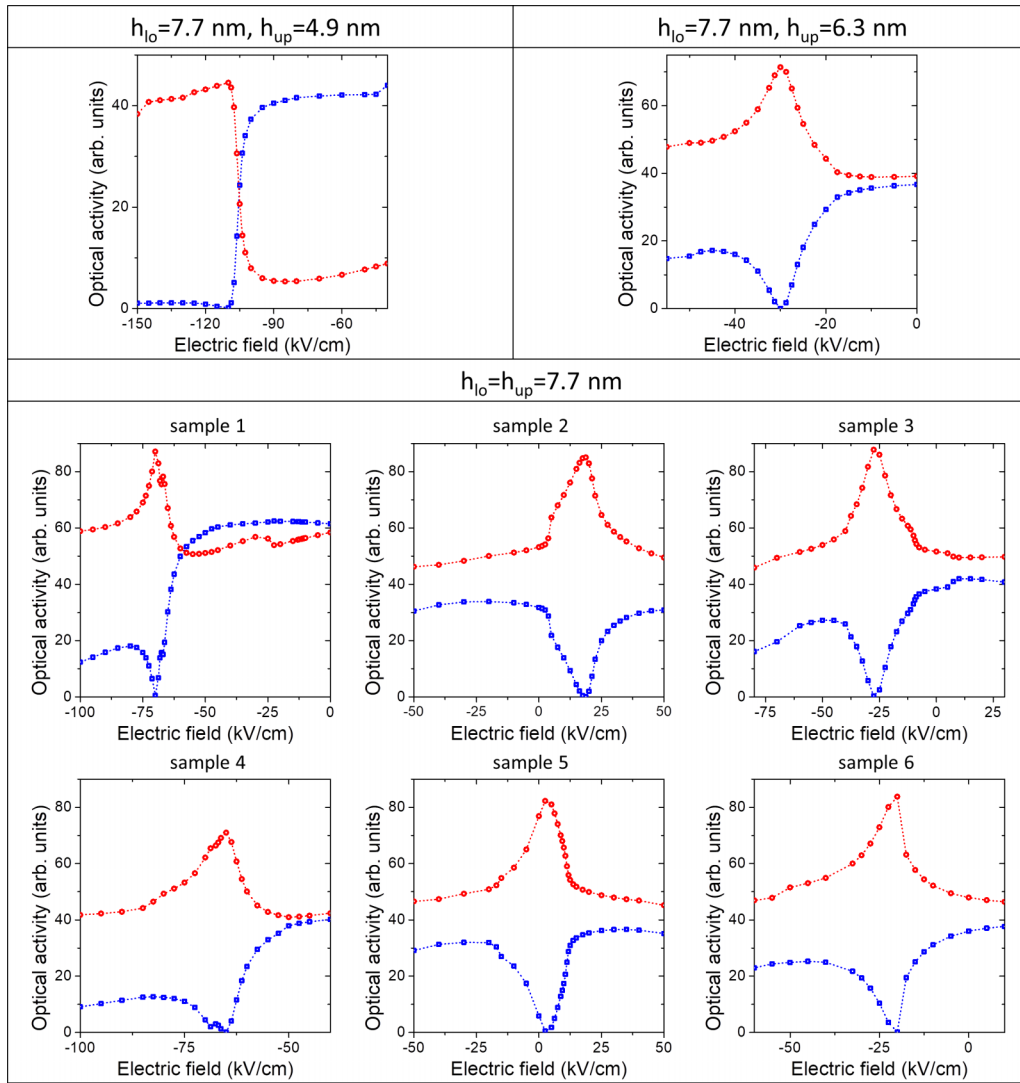
FIG. 12. Optical activities of lower (blue/light-gray squares) and higher (red/dark-gray circles) excitonic branches for various systems considered in this study. See the text for more details.

tonic states in Eq. (1) are given as linear combinations of four basis states, in the first case (of dissimilar heights), the optical activity is proportional to a squared modulus contribution from $|e_1 h_1, H/V\rangle$ states for H/V polarizations. However,

for delocalized electrons, it is (approximately) proportional to a squared modulus of the sum of expansion coefficients from $|e_1, h_1, H/V\rangle$ and $|e_1, h_2, H/V\rangle$ states (for H/V polarizations correspondingly) [43]. As shown in Figs. 13(b) and
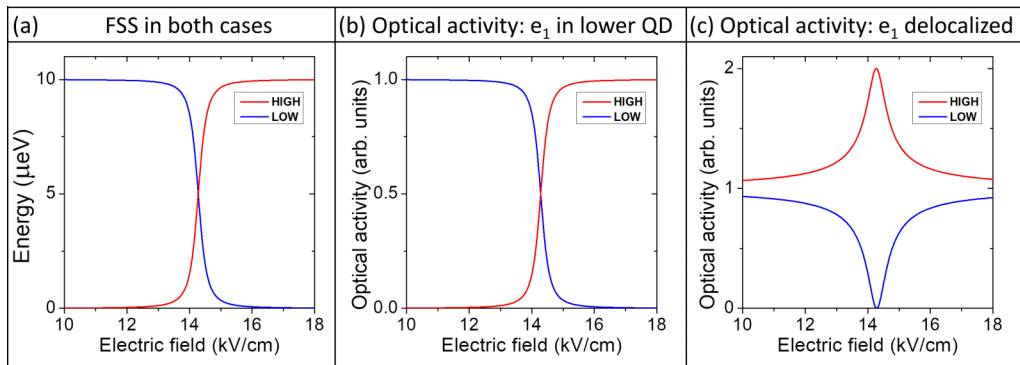

FIG. 13. (a) Bright-exciton splitting and optical activities of lower (blue/light-gray) and higher (red/dark-gray) excitonic branches for (b) a case where the ground-electron state (e_1) is localized in one dot and (c) delocalized over quantum dot molecules forming a bonding orbital.

13(c), this leads to entirely different optical spectra, despite an identical fine-structure evolution. In both cases, the coupling between the excitonic branches leads to a reduction in the lower-branch optical activity. However, for Fig. 13(c), there is a rebounce of lower-branch optical activity away from the crossing. In other words, the optical activity is inherently different, depending on the electron localization, as illustrated in Figs. 13(b) and 13(c) and shown earlier in the full atomistic calculations in Fig. 11 and Fig. 12. These results are consistent with effective mass modeling [43] of quantum dot molecules, where the tunneling of both electron and hole was determined as necessary to prevent degradation of optical activity of quantum dot molecules. However, in alloyed quantum dots, the fine structure splitting is dominated by randomness and is not introduced into modeling by means of auxiliary shape-elongation, and thus can strongly vary on a sample-to-sample basis, with some samples such tuning may not be easily achievable, despite favorable electron delocalization. Nonetheless, we found it is possible, for selected samples, with a vertical electric field, to reduce fine-structure splitting in alloyed nanowire quantum dot molecules without a detrimental reduction in optical activity.

V. SUMMARY AND DISCUSSION

We have shown the critical role of alloy randomness in the excitonic spectra of alloyed $InAs_{0.2}P_{0.8}$ nanowire quantum dot molecules. We started by discussing the results for quantum dot molecules formed by two coupled disk-shaped nanowire quantum dots of identical diameters and compositions, but notably different heights. In this case, where the difference of quantum dot heights dominates over alloy randomness, we recovered the usual direct-indirect exciton behavior, with lower and upper excitonic branches swapping their properties at the excitonic anticrossing.

However, if the difference in heights of quantum dots forming a molecule is small, then energy level fluctuations caused by randomness dominate, and the excitonic picture changes dramatically. To study this further, we consider six random realizations corresponding to nanowire quantum dot molecules built from quantum dots of the same height and composition, but with different arrangements on the atomic scale. We show that alloy randomness strongly affects hole-state localization, with the ground-hole state that can be localized in either of the dots or even form a delocalized (quasimolecular) orbital already at zero field. With the electron delocalized over both quantum dots, this leads to smearing of the traditional direct-indirect exciton notion, and peculiar behavior of the bright-exciton splitting at the level crossing is observed.

We found that in several random realizations, it is not possible to efficiently tune the fine-structure splitting below the 1 μeV threshold, with a rather peculiar and system-dependent field evolution that strongly varies for different random realizations. On the other hand, for several other random samples, the bright-exciton splitting of the lower branch can be tuned below 1 μeV while—due to strong electron delocalization—maintaining nonvanishing optical activity, with possible implications for quantum dot molecules applications in quantum information processing.

APPENDIX A: FIELD EVOLUTION OF PROBABILITY DENSITIES FOR DOUBLE QUANTUM DOTS WITH IDENTICAL HEIGHTS: ONE SAMPLE CASE

Figure 14 and Fig. 15 illustrate the electric-field evolution of ground and first-excited single-particle states, respectively, for one random realization of a quantum dot molecule formed by two quantum dots of identical height. The results presented here were obtained for sample 3; however, other samples showed qualitatively similar evolution except for ground-hole-state localization at zero field, as discussed in the main text. Because quantum dots have identical heights and we consider a large phosphorus content in the dot area, there is a pronounced coupling of electron states in the InP barrier, and thus, the coupling of the electron state forms quasimolecular e_1 and e_2 orbitals in the entire range of values considered in Fig. 14. However, similar to the case of quantum dots with dissimilar heights, the hole state remains well localized in their consistent dots and is coupled rather weakly in close vicinity of hole-state crossing, occurring for this particular sample at 6.25 kV/cm (Fig. 15).

APPENDIX B: SINGLE-PARTICLE FIELD EVOLUTION FOR DOUBLE QUANTUM DOTS WITH IDENTICAL HEIGHTS

For completeness, Fig. 16 shows the single-particle electric-field evolution of the electron and hole states for six random samples for a quantum dot molecule, built from two quantum dots of nominally identical dimensions. The electron-state evolution is virtually identical for all considered samples, whereas the hole-state evolution is quantitatively similar between samples, but with some quantitative differences, for example, different positions of hole resonance.

APPENDIX C: PARAMETERS OF THE PHENOMENOLOGICAL MODEL

Table IV lists the remaining fitting parameters used in the phenomenological model of Eq. (1) and discussed in the main text.

APPENDIX D: FURTHER SIMPLIFICATION OF A PHENOMENOLOGICAL MODEL

First, we focus only on the vicinity of excitonic crossing and set βs, γ_I, p_I, and S_I to zero. We also neglect δ_{DI} because it is very small. Nonetheless, we retain E_h, t, and p_D in $\mathbf{H}_1$ describing the hole-level crossing, and finally, derive two formulas for the fine excitonic splitting of low- and high-excitonic branches:
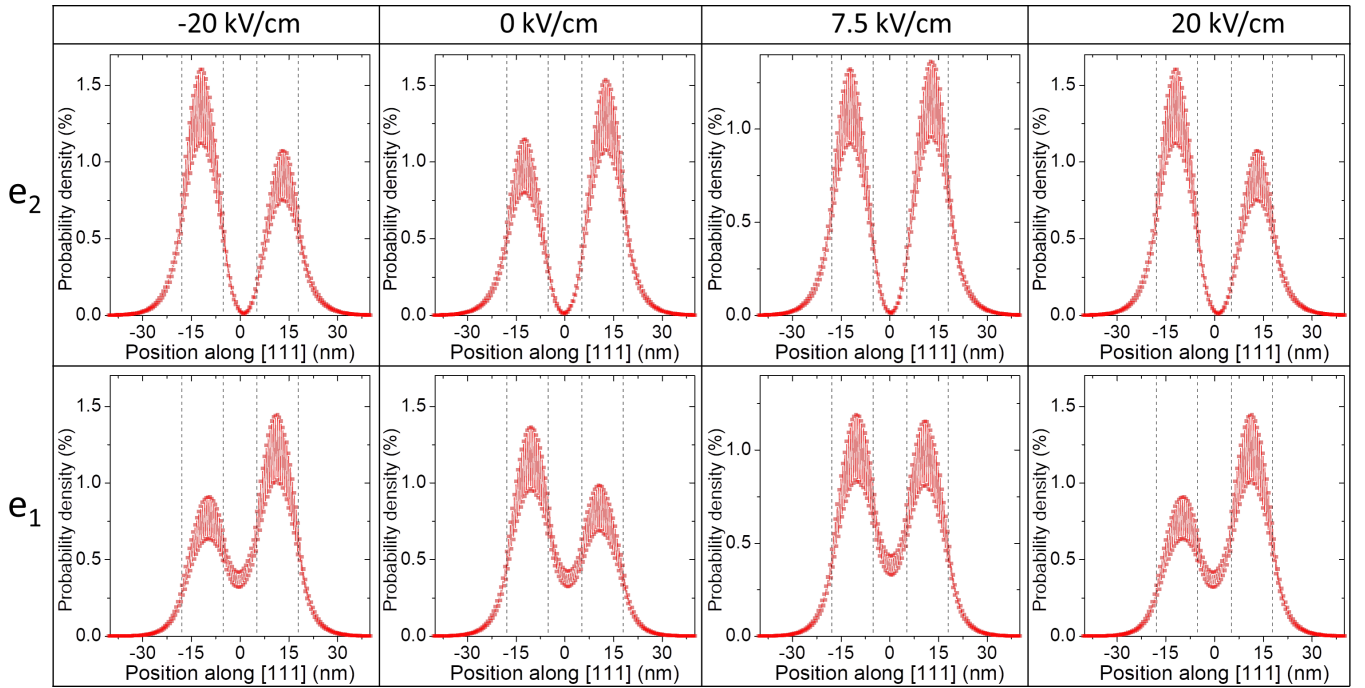
FIG. 14. Single-particle electron ground (e_1) and excited-state (e_2) probability densities (integrated over the lateral plane) for a nanowire quantum dot molecule formed by two alloyed $InAs_{0.2}P_{0.8}$ quantum dots of identical heights ($h_{down} = h_{up} = 7.7$), for several values of the external electric field, and as a function of position along the (vertical) growth [111] axis. Thin, vertical dashed lines indicate positions of individual quantum dots. Strong oscillatory characteristic is observed due to the presence of subsequent anion/cation monolayers. Strong coupling of electron states and formation of bonding and antibonding quasimolecular orbitals is apparent for all considered field values, particularly at electron-state anticrossing at 7.5 kV/cm.
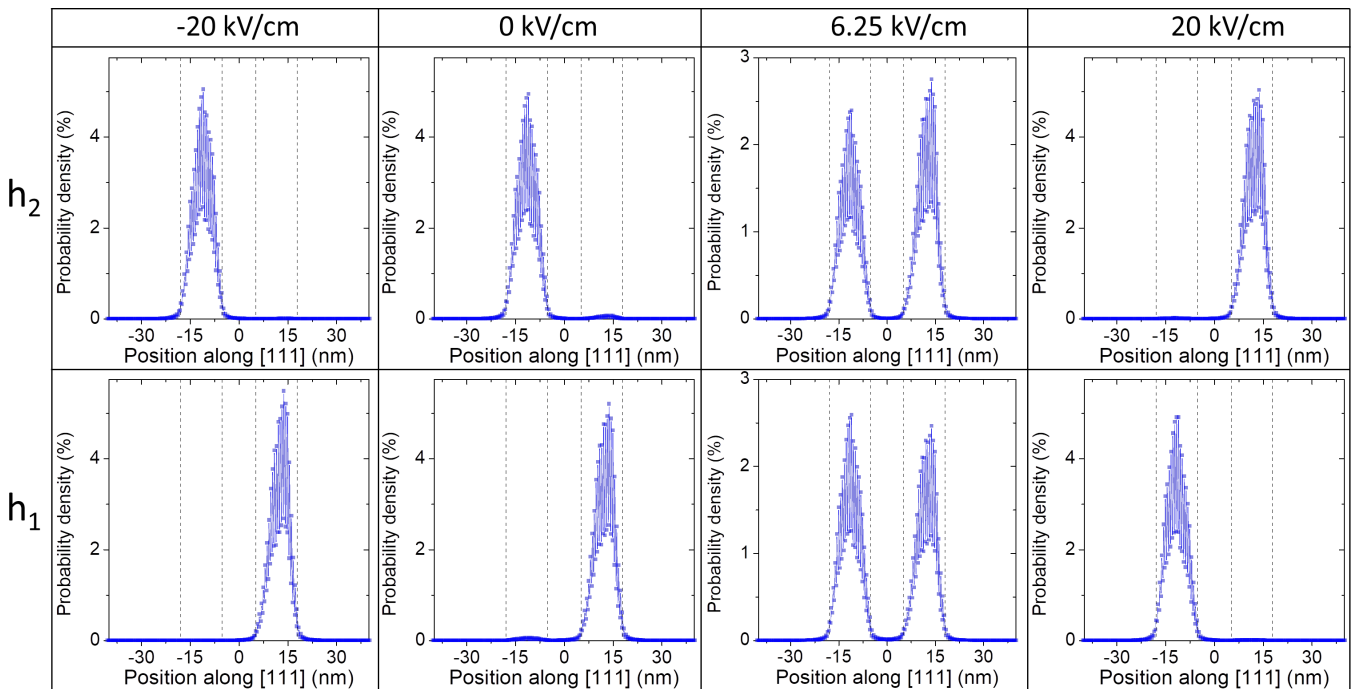

FIG. 15. Single-particle ground-hole (h_1) and excited-state (h_2) probability densities (integrated over the lateral plane) for a nanowire quantum dot molecule formed by two alloyed $InAs_{0.2}P_{0.8}$ quantum dots of identical heights ($h_{down} = h_{up} = 7.7$), for several values of the external electric field, and as a function of position along the (vertical) growth [111] axis. Thin, vertical dashed lines indicate positions of individual quantum dots. Strong oscillatory characteristic is observed due to the presence of subsequent anion/cation monolayers. Much stronger confinement is noted than in the case of electron states. At a field of 6.25 kV/cm, a pair of bonding and quasimolecular orbitals is formed, whereas for other field values, the hole states remain well localized in separate quantum dots.
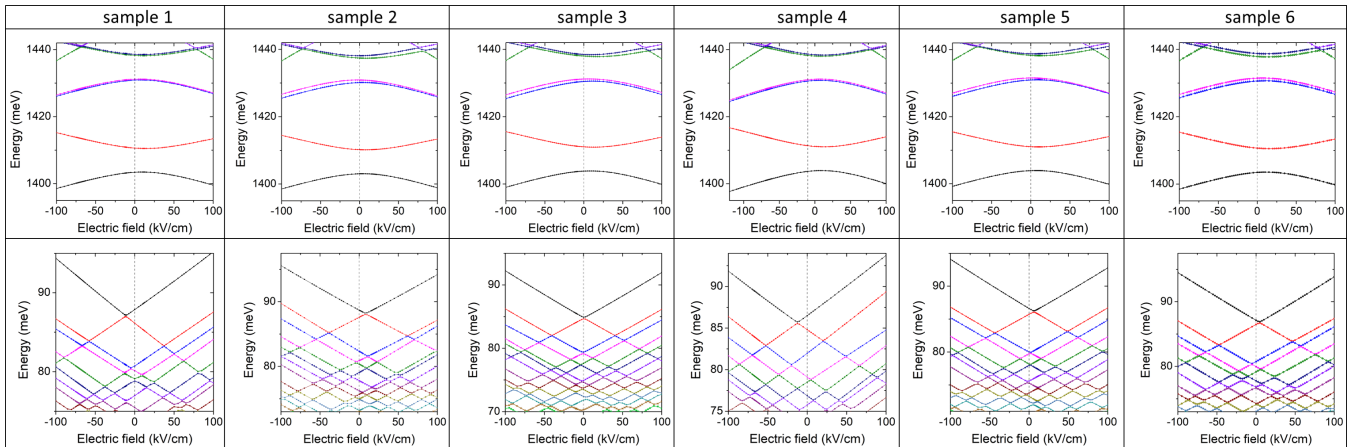
FIG. 16. Single-particle (upper row) electron and (lower row) hole spectra of the alloyed $InAs_{0.2}P_{0.8}$ nanowire quantum dot molecule formed from two quantum dots of identical heights ($h_{lo} = h_{up} = 7.7$), as a function of the external electric field. The vertical dashed black lines are guides to the eye for zero-field cases. Note the reverse ordering of the hole states and different vertical scales for the hole states.

$$\mathbf{FSS}_{low} = \tfrac{1}{2}|\gamma_D F - (S_D + S_I + \sqrt{(E_h + p_I F)^2 + 4t^2} - \sqrt{(\gamma_D F + E_h + p_I F + S_I - S_D)^2 + 4t^2})|$$

$$\mathbf{FSS}_{high} = \tfrac{1}{2}|\gamma_D F - (S_D + S_I - \sqrt{(E_h + p_I F)^2 + 4t^2} + \sqrt{(\gamma_D F + E_j + p_I F + S_I - S_D)^2 + 4t^2})|. \quad (D1)$$

Eq. (D1) confirms our earlier observation that the results are sensitive to the $S_I - S_D$ difference as well as the $h_2 - h_1$ difference (related to E_h and t [26,42]). As we focus on level splitting, the choice of E_X is irrelevant. Next, we further assume $S_D \gg S_I$ and that the $\gamma_D F$ term only weakly changes in the crossing region; thus, it is further neglected. Therefore, we retain S_D as the only parameter in the exchange $\mathbf{H}_2$ part of the Hamiltonian. In other words, we assume a "typical," well-pronounced excitonic branch anticrossing as in sample 1, as well as in double quantum dots of dissimilar sizes. In effect, we have the following simplified formulas for the excitonic fine structure:

$$\mathbf{FSS}_{low} = \tfrac{1}{2}|S_D + \sqrt{(E_h + p_I F)^2 + 4t^2} - \sqrt{(E_h + p_I F - S_D)^2 + 4t^2}|$$

$$\mathbf{FSS}_{high} = \tfrac{1}{2}|S_D - \sqrt{(E_h + p_I F)^2 + 4t^2} + \sqrt{(E_h + p_I F - S_D)^2 + 4t^2}| \quad (D2)$$

Next, we choose a set of exemplary parameters ($S = 10 \ \mu$eV, $E_h = 10$ meV, $t = 0.1$ meV, $p_I = 0.7 \times$ meVkV^{-1}cm), which we use to plot the results of Eq. (D2) in Fig. 13 (a) in the the main part of the text. Here, a particular choice of parameters is not relevant for the qualitative characteristic of the results, as long as they are chosen reasonably.

[1] M. T. Bjork, C. Thelander, A. Hansen, L. Jensen, M. Larsson, L. R. Wallenberg, and L. Samuelson, Few-electron quantum dots in nanowires, Nano Lett. **4**, 1621 (2004).

[2] M. T. Borgström, V. Zwiller, E. Müller, and A. Imamoglu, Optically bright quantum dots in single nanowires, Nano Lett. **5**, 1439 (2005).

[3] O. Benson, C. Santori, M. Pelton, and Y. Yamamoto, Regulated and Entangled Photons from a Single Quantum dot, Phys. Rev. Lett. **84**, 2513 (2000).

[4] R. M. Stevenson, R. J. Young, P. Atkinson, K. Cooper, D. A. Ritchie, and A. J. Shields, A semiconductor source of triggered entangled photon pairs, Nature (London) **439**, 179 (2006).

[5] B. W. Lovett, J. H. Reina, A. Nazir, and G. A. D. Briggs, Optical schemes for quantum computation in quantum dot molecules, Phys. Rev. B **68**, 205319 (2003).

[6] M. A. M. Versteegh, M. E. Reimer, K. D. Jöns, D. Dalacu, P. J. Poole, A. Gulinatti, A. Giudice, and V. Zwiller, Observation of strongly entangled photon pairs from a nanowire quantum dot, Nat. Commun. **5**, 5298 (2014).

[7] T. Huber, A. Predojevic, M. Khoshnegar, D. Dalacu, P. J. Poole, H. Majedi, and G. Weihs, Polarization entangled photons from quantum dots embedded in nanowires, Nano Lett. **14**, 7107 (2014).

[8] M. Prilmüller, T. Huber, M. Müller, P. Michler, G. Weihs, and A. Predojević, Hyperentanglement of Photons Emitted by a Quantum dot, Phys. Rev. Lett. **121**, 110503 (2018).

[9] M. Khoshnegar, T. Huber, A. Predojević, D. Dalacu, M. Prilmüller, J. Lapointe, X. Wu, P. Tamarat, B. Lounis, P. Poole *et al.*, A solid state source of photon triplets based on quantum dot molecules, Nat. Commun. **8**, 15716 (2017).

[10] R. S. Wagner and W. C. Ellis, Vapor-liquid-solid mechanism of single crystal growth, Appl. Phys. Lett. **4**, 89 (1964).

[11] L. E. Jensen, M. T. Björk, S. Jeppesen, A. I. Persson, B. J. Ohlsson, and L. Samuelson, Role of surface diffusion in chemical beam epitaxy of InAs nanowires, Nano Lett. **4**, 1961 (2004).

[12] D. Dalacu, A. Kam, D. G. Austing, X. Wu, J. Lapointe, G. C. Aers, and P. J. Poole, Selective-area vapour-liquid-solid growth of InP nanowires, Nanotechnology **20**, 395602 (2009).

[13] A. Fiset-Cyr, D. Dalacu, S. Haffouz, P. J. Poole, J. Lapointe, G. C. Aers, and R. L. Williams, In-situ tuning of individual position-controlled nanowire quantum dots via laser-induced intermixing, Appl. Phys. Lett. **113**, 053105 (2018).

[14] Y. Chen, I. E. Zadeh, K. D. Jöns, A. Fognini, M. E. Reimer, J. Zhang, D. Dalacu, P. J. Poole, F. Ding, V. Zwiller *et al.*, Controlling the exciton energy of a nanowire quantum dot by strain fields, Appl. Phys. Lett. **108**, 182103 (2016).

[15] S. Yanase, H. Sasakura, S. Hara, and J. Motohisa, Single-photon emission from inasp quantum dots embedded in density-controlled InP nanowires, Jpn. J. Appl. Phys. **56**, 04CP04 (2017).

[16] D. Dalacu, K. Mnaymneh, J. Lapointe, X. Wu, P. J. Poole, G. Bulgarini, V. Zwiller, and M. E. Reimer, Ultraclean emission from InAsP quantum dots in defect-free wurtzite InP nanowires, Nano Lett. **12**, 5919 (2012).

[17] M. Bouwes Bavinck, M. Zieliński, B. J. Witek, T. Zehender, E. P. A. M. Bakkers, and V. Zwiller, Controlling a nanowire quantum dot band gap using a straining dielectric envelope, Nano Lett. **12**, 6206 (2012).

[18] S. Haffouz, K. D. Zeuner, D. Dalacu, P. J. Poole, J. Lapointe, D. Poitras, K. Mnaymneh, X. Wu, M. Couillard, M. Korkusinski *et al.*, Bright single InAsP quantum dots at telecom wavelengths in position-controlled inp nanowires: The role of the photonic waveguide, Nano Lett. **18**, 3047 (2018).

[19] M. E. Reimer, G. Bulgarini, N. Akopian, M. Hocevar, M. B. Bavinck, M. A. Verheijen, E. P. A. M. Bakkers, L. P. Kouwenhoven, and V. Zwiller, Bright single-photon sources in bottom-up tailored nanowires, Nat. Commun. **3**, 737 (2012).

[20] M. van Weert, Quantum dots in vertical nanowire devices, Ph.D. thesis, Technische Universiteit Delft, The Netherlands, 2011.

[21] I. Vurgaftman, J. á. Meyer, and L. á. Ram-Mohan, Band parameters for iii–v compound semiconductors and their alloys, J. Appl. Phys. **89**, 5815 (2001).

[22] R. Singh and G. Bester, Lower Bound for the Excitonic Fine Structure Splitting in Self-Assembled Quantum dots, Phys. Rev. Lett. **104**, 196803 (2010).

[23] M. Gong, B. Hofer, E. Zallo, R. Trotta, J.-W. Luo, O. G. Schmidt, and C. Zhang, Statistical properties of exciton fine structure splitting and polarization angles in quantum dot ensembles, Phys. Rev. B **89**, 205312 (2014).

[24] M. Zieliński, Spectra of dark and bright excitons in alloyed nanowire quantum dots, Phys. Rev. B **100**, 045309 (2019).

[25] M. Zieliński, Excitonic complexes in InAs/InP nanowire quantum dots, Phys. Rev. B **101**, 195302 (2020).

[26] M. Świderski and M. Zieliński, Atomistic theory of excitonic fine structure in InAs/InP nanowire quantum dot molecules, Phys. Rev. B **95**, 125407 (2017).

[27] P. Michler, *Quantum Dots for Quantum Information Technologies*, Vol. 237 (Springer, Cham, 2017).

[28] M. Świderski and M. Zieliński, Electric field tuning of excitonic fine-structure splitting in asymmetric InAs/InP nanowire quantum dot molecules, Phys. Rev. B **100**, 235417 (2019).

[29] M. Bayer, P. Hawrylak, K. Hinzer, S. Fafard, M. Korkusinski, Z. R. Wasilewski, O. Stern, and A. Forchel, Coupling and entangling of quantum states in quantum dot molecules, Science **291**, 451 (2001).

[30] J. Wu and Z. M. Wang, *Quantum Dot Molecules* (Springer, New York, 2014).

[31] M. Scheibner, A. S. Bracker, D. Kim, and D. Gammon, Essential concepts in the optical properties of quantum dot molecules, Solid State Commun. **149**, 1427 (2009), fundamental Phenomena and Applications of Quantum Dots.

[32] M. F. Doty, J. I. Climente, M. Korkusinski, M. Scheibner, A. S. Bracker, P. Hawrylak, and D. Gammon, Antibonding Ground States in Inas Quantum-dot Molecules, Phys. Rev. Lett. **102**, 047401 (2009).

[33] W. Jaskólski, M. Zieliński, G. W. Bryant, and J. Aizpurua, Strain effects on the electronic structure of strongly coupled self-assembled InAs/GaAs quantum dots: Tight-binding approach, Phys. Rev. B **74**, 195339 (2006).

[34] G. Bester, A. Zunger, and J. Shumway, Broken symmetry and quantum entanglement of an exciton in $In_xGa_{1-x}As$/GaAs quantum dot molecules, Phys. Rev. B **71**, 075325 (2005).

[35] J. Planelles, F. Rajadell, and J. I. Climente, Symmetry-induced hole-spin mixing in quantum dot molecules, Phys. Rev. B **92**, 041302 (2015).

[36] M. F. Doty, J. I. Climente, A. Greilich, M. Yakes, A. S. Bracker, and D. Gammon, Hole-spin mixing in inas quantum dot molecules, Phys. Rev. B **81**, 035308 (2010).

[37] P. L. Ardelt, K. Gawarecki, K. Müller, A. M. Waeber, A. Bechtold, K. Oberhofer, J. M. Daniels, F. Klotz, M. Bichler, T. Kuhn, H. J. Krenner, P. Machnikowski, and J. J. Finley, Coulomb Mediated Hybridization of Excitons in Coupled Quantum dots, Phys. Rev. Lett. **116**, 077401 (2016).

[38] H. J. Krenner, M. Sabathil, E. C. Clark, A. Kress, D. Schuh, M. Bichler, G. Abstreiter, and J. J. Finley, Direct Observation of Controlled Coupling in an Individual Quantum dot Molecule, Phys. Rev. Lett. **94**, 057402 (2005).

[39] E. A. Stinaff, M. Scheibner, A. S. Bracker, I. V. Ponomarev, V. L. Korenev, M. E. Ware, M. F. Doty, T. L. Reinecke, and D. Gammon, Optical signatures of coupled quantum dots, Science **311**, 636 (2006).

[40] M. Scheibner, M. F. Doty, I. V. Ponomarev, A. S. Bracker, E. A. Stinaff, V. L. Korenev, T. L. Reinecke, and D. Gammon, Spin fine structure of optically excited quantum dot molecules, Phys. Rev. B **75**, 245318 (2007).

[41] M. F. Doty, M. Scheibner, I. V. Ponomarev, E. A. Stinaff, A. S. Bracker, V. L. Korenev, T. L. Reinecke, and D. Gammon, Electrically Tunable *g* Factors in Quantum dot Molecular Spin States, Phys. Rev. Lett. **97**, 197202 (2006).

[42] N. Sköld, A. Boyer de la Giroday, A. J. Bennett, I. Farrer, D. A. Ritchie, and A. J. Shields, Electrical Control of the Exciton Fine Structure of a Quantum dot Molecule, Phys. Rev. Lett. **110**, 016804 (2013).

[43] H. Y. Ramírez and S.-J. Cheng, Tunneling Effects on Fine-Structure Splitting in Quantum-dot Molecules, Phys. Rev. Lett. **104**, 206402 (2010).

[44] M. Scheibner, S. E. Economou, A. S. Bracker, D. Gammon, and I. V. Ponomarev, Entangled photon pair generation with quantum dot molecules, J. Opt. Soc. Am. B **29**, A82 (2012).

[45] C. Jennings and M. Scheibner, Entanglement dynamics of molecular exciton states in coupled quantum dots, Phys. Rev. B **93**, 115311 (2016).

[46] P. Schillak, Excitonic states and photoluminescence spectra of a quantum dot molecule exposed to the external static electric field, Phys. Status Solidi B **255**, 1800231 (2018).

[47] P. N. Keating, Effect of invariance requirements on the elastic strain energy of crystals with application to the diamond structure, Phys. Rev. **145**, 637 (1966).

[48] R. M. Martin, Elastic properties of ZnS structure semiconductors, Phys. Rev. B **1**, 4005 (1970).

[49] T. Saito and Y. Arakawa, Electronic structure of piezoelectric $In_0.2Ga_0.8N$ quantum dots in gan calculated using a tight-binding method, Physica E **15**, 169 (2002).

[50] J.-M. Jancu, R. Scholz, F. Beltram, and F. Bassani, Empirical spds* tight-binding calculation for cubic semiconductors: General method and material parameters, Phys. Rev. B **57**, 6493 (1998).

[51] D. J. Chadi, Spin-orbit splitting in crystalline and compositionally disordered semiconductors, Phys. Rev. B **16**, 790 (1977).

[52] M. Zieliński, Including strain in atomistic tight-binding hamiltonians: An application to self-assembled InAs/GaAs and InAs/InP quantum dots, Phys. Rev. B **86**, 115424 (2012).

[53] M. Zieliński, Valence band offset, strain and shape effects on confined states in self-assembled InAs/InP and InAs/GaAs quantum dots, J. Phys.: Condens. Matter **25**, 465301 (2013).

[54] S. Lee, F. Oyafuso, P. von Allmen, and G. Klimeck, Boundary conditions for the electronic structure of finite-extent embedded semiconductor nanostructures, Phys. Rev. B **69**, 045316 (2004).

[55] M. Zieliński, Multi-scale simulations of semiconductor nanostructures, Acta Phys. Pol. A **122**, 312 (2012).

[56] M. Zieliński, M. Korkusinski, and P. Hawrylak, Atomistic tight-binding theory of multiexciton complexes in a self-assembled inas quantum dot, Phys. Rev. B **81**, 085301 (2010).

[57] T. P. Sheerin, D. S. P. Tanner, and S. Schulz, Atomistic analysis of piezoelectric potential fluctuations in zinc-blende ingan/gan quantum wells: A stillinger-weber potential based analysis, Phys. Rev. B **103**, 165201 (2021).

[58] M. Gong, K. Duan, C.-F. Li, R. Magri, G. A. Narvaez, and L. He, Electronic structure of self-assembled InAs/InP quantum dots: Comparison with self-assembled InAs/GaAs quantum dots, Phys. Rev. B **77**, 045326 (2008).

[59] X. Ma, G. W. Bryant, and M. F. Doty, Hole spins in an InAs/GaAs quantum dot molecule subject to lateral electric fields, Phys. Rev. B **93**, 245402 (2016).

[60] Edited by P. Michler, *Single Quantum Dots: Fundamentals, Applications and New Concepts*, Vol. 90 (Springer, New York, 2003).

[61] S. Lee, L. Jönsson, J. W. Wilkins, G. W. Bryant, and G. Klimeck, Electron-hole correlations in semiconductor quantum dots with tight-binding wave functions, Phys. Rev. B **63**, 195318 (2001).

[62] S. Schulz, S. Schumacher, and G. Czycholl, Tight-binding model for semiconductor quantum dots with a wurtzite crystal structure: From one-particle properties to coulomb correlations and optical spectra, Phys. Rev. B **73**, 245327 (2006).

[63] P. T. Różański and M. Zieliński, Linear scaling approach for atomistic calculation of excitonic properties of 10-million-atom nanostructures, Phys. Rev. B **94**, 045440 (2016).

[64] P. T. Różański and M. Zieliński, Efficient computation of coulomb and exchange integrals for multi-million atom nanostructures, Comput. Phys. Commun. **238**, 254 (2019).

[65] M. Świderski and M. Zieliński, Exact diagonalization approach for atomistic calculation of piezoelectric effects in semiconductor quantum dots, Acta Phys. Pol. A **129**, A-79 (2016).

[66] T. Warming, E. Siebert, A. Schliwa, E. Stock, R. Zimmermann, and D. Bimberg, Hole-hole and electron-hole exchange interactions in single InAs/GaAs quantum dots, Phys. Rev. B **79**, 125316 (2009).

[67] N. Liu, J. Tersoff, O. Baklenov, A. L. Holmes, and C. K. Shih, Nonuniform Composition Profile in $In_{0.5}Ga_{0.5}As$ Alloy Quantum dots, Phys. Rev. Lett. **84**, 334 (2000).

[68] A. J. Williamson, L. W. Wang, and A. Zunger, Theoretical interpretation of the experimental electronic structure of lens-shaped self-assembled InAs/GaAs quantum dots, Phys. Rev. B **62**, 12963 (2000).

[69] W. Sheng and P. Hawrylak, Spin polarization in self-assembled quantum dots, Phys. Rev. B **73**, 125331 (2006).

[70] M. S. Dresselhaus, G. Dresselhaus, and A. Jorio, *Group Theory: Application to the Physics of Condensed Matter* (Springer Science & Business Media, Berlin, Heidelberg, 2007).

[71] M. Bayer, G. Ortner, O. Stern, A. Kuther, A. A. Gorbunov, A. Forchel, P. Hawrylak, S. Fafard, K. Hinzer, T. L. Reinecke, S. N. Walck, J. P. Reithmaier, F. Klopf, and F. Schäfer, Fine structure of neutral and charged excitons in self-assembled In(Ga)As/(Al)GaAs quantum dots, Phys. Rev. B **65**, 195315 (2002).

[72] M. Zieliński, Dark-bright excitons mixing in alloyed ingaas self-assembled quantum dots, Phys. Rev. B **103**, 155418 (2021).

[73] A. Bennett, M. Pooley, R. Stevenson, M. Ward, R. Patel, A. B. de La Giroday, N. Sköld, I. Farrer, C. Nicoll, D. Ritchie *et al.*, Electric-field-induced coherent coupling of the exciton states in a single quantum dot, Nat. Phys. **6**, 947 (2010).

[74] R. Singh and G. Bester, Nanowire Quantum dots as An Ideal Source of Entangled Photon Pairs, Phys. Rev. Lett. **103**, 063601 (2009).

[75] T. Eissfeller, Theory of the electronic structure of quantum dots in external fields, Ph.D. thesis, Technical University of Munich, 2012.

[76] M. Korkusinski and P. Hawrylak, Atomistic theory of emission from dark excitons in self-assembled quantum dots, Phys. Rev. B **87**, 115310 (2013).

[77] L. Jacak, P. Hawrylak, and A. Wojs, *Quantum Dots* (Springer, Berlin, 1998).

[78] M. Zieliński, From quantum dots to quantum dashes: Excitonic spectra of highly elongated InAs/InP nanostructures, Phys. Rev. B **99**, 205402 (2019).

[79] MATLAB, *version 8.2.0.701 (R2013b)* (The MathWorks Inc., Natick, Massachusetts, 2013).